The biochemical basis for the cooperative action of microRNAs

By

Daniel Briskin

B.S., Molecular Genetics (2012)
Ohio State University

SUBMITTED TO THE DEPARTMENT OF BIOLOGY IN PARTIAL FULFILLMENT OF
THE REQUIREMENTS FOR THE DEGREE OF

DOCTOR OF PHILOSOPHY
AT THE
MASSACHUSETTS INSTITUTE OF TECHNOLOGY

SEPTEMBER 2019 [February 2020]

Signature redacted

Signature of Author:
Daniel Briskin
Department of Biology
17 September 2019

Signature redacted

Certified By:
David P. Bartel
Professor of Biology
Thesis Supervisor

Signature redacted

Accepted By:
Stephen Bell
Uncas and Helen Whitaker Professor of Biology
Investigator, Howard Hughes Medical Institute
Co-Director, Biology Graduate Committee

1

The biochemical basis for the cooperative action of microRNAs

by

Daniel Briskin

Submitted to the Department of Biology on 17 September 2019
In partial fulfillment of the requirements for the degree of doctor of philosophy

Abstract

In metazoans, microRNAs (miRNAs) act to repress mRNAs through a combination of translational repression and target degradation. miRNAs predominantly pair within the 3′ untranslated region (3′ UTR) of the mRNA. In cells, closely spaced miRNA target sites within an mRNA can act cooperatively, leading to more repression of the target mRNA than expected by independent action at each site.

This dissertation details the use of purified miRNA–AGO2 complexes, synthetic target RNAs, and a purified domain of TNRC6B that is able to simultaneously bind multiple AGO proteins. We examined the target site occupancy and affinities for miRNA–AGO2 binding in the absence and presence of TNRC6B, for target RNAs with a single miRNA site as well as multiple miRNA sites spaced at varying distances. As miRNA–AGO-binding to target correlates with target repression, our study assayed target binding.

Absent TNRC6B, miRNA–AGO2 complexes showed little if any cooperative binding. In the presence of the AGO-binding domain of TNRC6B, we observed strong cooperative binding to dual-site target RNAs. We went on to explore the miRNA site parameters suitable for cooperativity, investigating the spacing between sites as well as different miRNAs working alone or in combination with one another. To interrogate the mechanism by which TNRC6B increases cooperativity, competitive slicing experiments were performed; results indicated that association rates between miRNA–AGO2 complexes and targets were not affected by TNRC6B, which implied that the improved affinities were due to reduced dissociation. Thus, the multivalent binding of TNRC6 enables cooperative binding of miRNA–AGO complexes to target RNAs, thereby explaining the basis of cooperative action.

Thesis advisor: David P. Bartel
Title: Professor

Acknowledgments

I have been fortunate to work with a special group of people over the past five years of my graduate studies. First, I would like to thank Dave Bartel for his scientific guidance and rigor. Thanks to my thesis committee, Tom RajBhandary and Phil Sharp, for their guidance and support on my project. I would also like to thank the above group of people for their instruction in the courses 7.77 and 7.60, where even before joining a lab I learned to think more deeply about the RNA-centric questions that interested me. Thank you to Gianpiero DiLeva, my first scientific mentor, who started to teach me how to think about and do science. Finally, I am sincerely grateful to Tom Tuschl, under whom I had the pleasure of working for two years as a technician. Tom is the person who got me excited about science; working in his lab, I began to understand the thrills of what research could illuminate and the impact that research can have outside of the lab.

I would also like to thank other members of the Bartel lab. Laura and Asia are the backbone of the lab who keep the day-to-day aspects running as smoothly as they do. Laura has, on more than one occasion, helped me to rush a rad order, allowing me to complete some critical, last experiment before lab meeting. Asia wrangles the cornucopia of equipment we have in the lab, some component of which is always breaking down. Nonetheless, she works to make sure that we always have whatever we need to do our work. (Furthermore, she takes on the daunting task of interfacing with the vendors.) I also thank Bartel lab graduate students, postdocs, and technicians. The attention that lab mates give to each others' projects is exceptional; I have received help from all of my peers and to them I am deeply grateful. Thanks, Papa Sean, my blood brother. I would also like to specifically thank my friends in 623, Tim, Jamie McKwasnieski, Michael, (Glenn and Emir, RIP) and my bay mate Matt. They make 623 the most fun room in Bartel lab. From discussing science, to double blocks, I always looked forward to coming in and talking about what is happening in our lives and the world. I'd like to thank and "thank" Matt for encouraging my running. It's the most fun and rewarding aspect of my life, but also responsible for an unfortunate number of trips to MIT Medical. I'd also like to thank Breakfast Club (Elena) for a friendly way to start the day. Thanks, Swim Club (paradoxically, the most exclusive and least elite swim team in the world), for giving me one less way to die. And thank you to Run Club for traveling near and far to run beautiful and challenging courses.

I'd like to thank my classmates Laurens and Nolan for their friendship over the years. Thank you to ~~dead to me people~~ ~~classmates~~ ~~housemates~~ friends at 6 Antrim St., Chris, Grace, John, Josh, Santi, and Spencer. They have been an exceptional group of people to joke, commiserate, and live with. I have learned a multitude from these friends: from what lawyers are, to Caligula's travails, to being more woke, and to naht take my half out of the middle. I can always count on them to slap some sense into me.

My family, Jeanne, Dan, Joe, Lily, Jackie, Ken, Olivia, Grandma, Grandpa, Benjamin, Emily, Mom and Dad, for your unwavering love and support, I love and thank you.

Table of contents

Chapter 1. Introduction

miRNA biogenesis

MicroRNAs (miRNAs) are short, non-coding RNAs approximately 22 nucleotides (nt) long that complex with Argonaute (AGO) proteins to posttranscriptionally regulate target gene expression through a combination of translational repression and mRNA destabilization. miRNAs target mRNAs through Watson–Crick pairing between the miRNA and mRNA target at sites typically within the 3′ untranslated region (3′ UTR) of the mRNA. AGO proteins mediate mRNA degradation through three distinct mechanisms. One mechanism, unique to AGO2, one of four AGO paralogues in mammals, is using its catalytically active RNase H-like domain that, upon extensive complementarity between the miRNA guide and target mRNA, is used to cleave, or slice, the target, leading to the target's degradation (Elbashir et al., 2001; Schirle and MacRae, 2012; Song et al., 2004). The other human AGO paralogues, AGO1, 3, and 4, are loaded with miRNAs but do not cleave their targets (Liu et al., 2004; Meister et al., 2004). In addition, the vast majority of miRNAs do not pair extensively enough with their target as required to induce cleavage but rather bind with complementarity to the miRNA seed region (miRNA nucleotides 2–7) (Bartel, 2009). These non-cleavage competent interactions repress mRNA through other modes: translational repression and mRNA destabilization.

Early characterization of miRNAs was done in *C. elegans* where the *lin-4* gene was found to regulate *lin-14* activity, which plays a role in *C. elegans* development (Lee et al., 1993; Wightman et al., 1993). The product of *lin-4* is not a protein but rather a 21

9

nt RNA with complementarity to multiple sites in the 3′ UTR of *lin-14*. Since this early

work, miRNAs have been found throughout eukaryotes, including plants and animals

(Bartel, 2004; Lagos-Quintana et al., 2001).

In metazoans, canonical miRNAs are transcribed by RNA polymerase II as part

of a primary transcript that is capped and polyadenylated (Fig. 1) (Cai et al., 2004; Lee

et al., 2004). miRNAs may be found in the transcribed sequence of protein-coding

genes, typically in introns, or have their own promoters (Ha and Kim, 2014). The

primary miRNA transcript (pri-miRNA) has regions of sequence with reverse

complementarity such that the RNA folds back on itself and makes a stem-loop. This

stem-loop is then processed by a heterotrimeric complex called microprocessor,

consisting of two DiGeorge syndrome critical region 8 (DGCR8) proteins and one

Drosha. DGCR8 acts as a cofactor for Drosha, which has two RNase III domains, each

of which interacts with one DGCR8 (Kwon et al., 2016). One RNase III domain cleaves

the 5′ strand of the stem-loop; the other RNase III domain cleaves the 3′ strand of the

stem-loop (Han et al., 2004). Features that improve processing of pri-miRNAs include

both structural and primary sequence elements (Fang and Bartel, 2015). Structurally,

pri-miRNA processing is favored by a 35 base pair (bp) stem length with an apical loop

of ≥10 nt and basal single stranded RNA (Fang and Bartel, 2015). Drosha functions as

a ruler to measure 11 bp from the basal junction for one cut site; cutting both strands of

RNA duplex produces a hairpin with a 5′ phosphate and 2 nt 3′ hydroxy overhang; this

species is known as the pre-miRNA (Kwon et al., 2016). The pre-miRNA is then

exported from the nucleus by exportin 5 in complex with RAN–GTP (Lund et al., 2004; Yi et al., 2003).

Once in the cytoplasm, the pre-miRNA is processed by Dicer. Dicer recognizes the 5' and 3' ends of the pre-miRNA and cleaves the pre-miRNA at two places to generate an RNA duplex typified by two ~22 nt RNA molecules, each with 5' phosphate and 3' hydroxy termini and a 2 nt 3' overhang on each end (Bernstein et al., 2001; Hutvagner et al., 2001; Park et al., 2011; Tian et al., 2014; Zhang et al., 2002). Finally, one of the two strands of RNA is loaded into AGO. The more unstable 5' end of the duplex is favored for AGO loading (Khvorova et al., 2003; Schwarz et al., 2003). Additionally, AGO favors loading strands with 5' adenosine or 5' uridine (Suzuki et al., 2015). However, some duplexes exhibit essentially equal loading between the originally 5' and 3' strands, which become the 5p and 3p strands, respectively. The strand that is loaded into AGO is termed the guide strand, while the strand that is not loaded is termed the passenger, or star, strand. The unloaded strand is degraded by endogenous RNases.
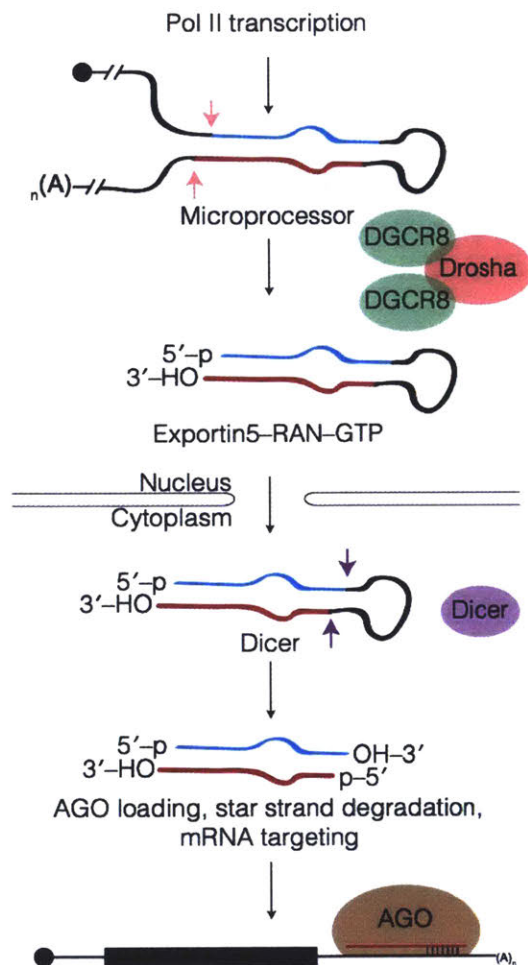
Figure 1. miRNA biogenesis
miRNAs are transcribed by RNA polymerase II, resulting in a capped and polyadenylated transcript. Drosha (salmon) works in combination with two DGCR8 (green) to cleave the pri-miRNA at indicated sites (salmon arrows) to generate the pre-miRNA. Exportin5–RAN–GTP exports the pre-miRNA from the nucleus to the cytoplasm where Dicer (purple) further cleaves (purple arrows) to generate the mature miRNA. Finally, the guide miRNA strand (red) is loaded into AGO protein (brown) to target an mRNA (black). The passenger strand (blue) is degraded.

Some miRNAs are processed in a Dicer-independent way, such as miR-451.

miR-451 is transcribed as a relatively short hairpin such that it is too short for proper

Dicer processing (Siolas et al., 2005). Thus, the hairpin is loaded directly into an AGO,

although AGO2 is uniquely capable of processing the miR-451 due to the catalytic

domain of AGO2. The hairpin is cleaved by AGO2, the short 3′ cleavage fragment is

ejected, and the 3′ end of the loaded miRNA is trimmed back by endogenous nucleases

(Cheloufi et al., 2010; Cifuentes et al., 2010; Yoda et al., 2013). Similarly, miR-486,

although Dicer dependent, requires AGO2 catalytic activity to slice and eject the guide

strand to generate mature miR-486–AGO2 (Jee et al., 2018).

Argonaute proteins are divided into four globular domains, termed N, MID, PIWI,

and PAZ, and two linker domains, L1 and L2 (Song et al., 2004; Swarts et al., 2014b).

The 5′ terminus of the miRNA is tethered to the MID domain of AGO (Elkayam et al.,

2012; Ma et al., 2005; Parker et al., 2005; Schirle and MacRae, 2012). The 5′

nucleotide inserts into a binding pocket on AGO such that it is not available for target

pairing (Elkayam et al., 2012; Ma et al., 2005; Schirle et al., 2015; Wang et al., 2009).

Target mRNAs often have an adenosine at their first position, and this base specifically

goes into a pocket between the MID and L2 domains (Lewis et al., 2005; Schirle et al.,

2015; Schirle et al., 2014). Nucleotides 2–6 of the guide RNA are prearranged in A-form

helix and exposed to the solvent, which helps speed miRNA target searching (Bartel,

2018; Chandradoss et al., 2015; Elkayam et al., 2012; Salomon et al., 2015; Schirle and

MacRae, 2012). Not only does AGO confer shape to and nuclease protection upon the

loaded miRNA, but the loaded miRNA also confers stability upon AGO, increasing AGO

resistance to protease (Elkayam et al., 2012). Only limited interactions are observed

between AGO and the Watson–Crick face of nucleotides, but interactions are observed

with the backbone of the miRNA, including Van der Waals interactions with the 2′ hydroxy of the ribose (Schirle and MacRae, 2012).

The PIWI domain of AGO contains the active site DEDH tetrad reminiscent of RNase H enzymes, which uses Mg^{2+} as a cofactor (Liu et al., 2004; Nakanishi et al., 2012). Although AGO2 is considered the only biological catalytically active of the four human paralogues, AGO3 has the same four amino acid residues in its catalytic tetrad as AGO2 and, under the right guide–target sequence conditions, AGO3 can catalyze cleavage of target RNA, albeit less effectively than AGO2 (Park et al., 2017). The greatly reduced cleavage activity of AGO3 is due to an immature, or less rigidly structured, nucleic acid binding channel between the N and PIWI domains (Hauptmann et al., 2013; Park et al., 2017). AGO1 does not conserve the catalytic tetrad of AGO2 (inactive DEDR in AGO1 rather than the active DEDH of AGO2) and therefore cannot slice target (Faehnle et al., 2013; Nakanishi et al., 2013). AGO4 is also incapable of slicing target, having a catalytically inactive DEGR at the would-be active site (Park et al., 2019).

The central region of miRNAs can be largely unpaired from target, even given complementarity to target (Sheu-Gruttadauria et al., 2019). Indeed, AGO can accommodate a bridge of up to 15 upaired target nucleotides across from the central region of a miRNA while still effectively repressing target (Sheu-Gruttadauria et al., 2019). The 3′ half of the miRNA interacts with the PAZ domain of AGO. Guide nucleotides 14–18 are fed through a channel between the PAZ and N domains. miRNA–AGO interactions perturb base stacking; the Watson-Crick edges of guide

nucleotides 15, 17, and 18 face toward AGO, away from the solvent, and are therefore unavailable for target pairing in the solved structure (Schirle et al., 2014). Supplemental pairing, pairing of miRNA nucleotides 13–16 to target mRNA, requires a conformational change in AGO whereby guide nucleotides 13–16 are exposed for pairing and a supplementary chamber of AGO is opened to accommodate base pairing to target (Sheu-Gruttadauria et al., 2019).

miRNA-mediated target repression mechanism

The mammalian miRNA–AGO complex targets mRNAs, typically in the 3′ UTR, through complementary base pairing. Compared to naked RNA, AGO increases the association rate, k_{on}, of miRNA pairing with target (Salomon et al., 2015). This increase in k_{on} is executed by AGO structurally prearranging seed of the loaded miRNA into an A-form helix (Bartel, 2018; Elkayam et al., 2012; Schirle and MacRae, 2012). Although AGO increases k_{on}, of miRNA to target, it also increases dissociation rate, k_{off} of fully paired target, relative to naked RNA pairing (Wee et al., 2012). Overall, miRNA–AGO has lower affinity for target RNA in comparison to the pairing of two naked RNA molecules (Salomon et al., 2015; Wee et al., 2012).

More than 60% of human mRNAs have conserved target sites of miRNAs (Friedman et al., 2009). Like many genes, miRNA expression is temporally and spatially regulated (Landgraf et al., 2007). The more productive canonical mammalian miRNA target sites have 6–7 nt of contiguous base pairing, including nucleotides 2–7 or 2–8 of the miRNA (termed 6mer and 7mer-m8 sites, respectively) (Fig. 2) (Bartel, 2009, 2018).

15

If the target mRNA has an adenosine residue across from position 1 of the miRNA and nucleotides 2–7 or 2–8 are paired, the sites, respectively, are called a 7mer-A1 or 8mer. Other miRNA–target pairing regimes include supplementary pairing, which often includes pairing across from nucleotides 13–16 of the miRNA, and compensatory pairing, in which imperfect pairing to the miRNA seed can be somewhat compensated for by additional pairing to the 3′ region of the miRNA often including nucleotides 13–16 (Brennecke et al., 2005; Doench and Sharp, 2004; Grimson et al., 2007).

```
                          Seed
                        87654321
              3'-NNNNNNNNNNNNNNNNNNNNNN-5'      miRNA
                                 | | | | | | |
    8mer  5'...NNNNNNNNNNNNNNNNNNNNNNNNNNNANN...3'|mRNA
    7mer-m8 5'...NNNNNNNNNNNNNNNNNNNNNNNNNNNBNN...3'|
    7mer-A1 5'...NNNNNNNNNNNNNNNNNNNNNNNNNNNANN...3'|
    6mer  5'...NNNNNNNNNNNNNNNNNNNNNNNNNNNBNN...3'|

                          Seed
                        87654321
              3'-NNNNNNNNNNNNNNNNNNNNNN-5'      miRNA
                    | | | |       | | | | | | |
3' Supplementary 5'...NNNNNNNNNNNNNNNNNNNNNNNNNNNNNN...3' mRNA

                          Seed
                        87654321
              3'-NNNNNNNNNNNNNNNNNNNNNN-5'      miRNA
                    | | | |      | |  | | | |
3' Compensatory 5'...NNNNNNNNNNNNNNNNNNNNNNNNNNNNNN...3' mRNA
```

Figure 2. miRNA–mRNA target site types
The miRNA (top) is shown with its seed (red) base paired to target mRNA. In cells, the miRNA is loaded into an Argonaute protein (not shown). For various mRNA pairing sites, the nucleotides involved in base pairing are diagramed in blue. 8mer, 7mer-m8, 7mer-A1, and 6mer sites are canonical site types diagramed in descending order of pairing stability. 3′ supplementary and compensatory sites are atypical and are diagramed in descending order of pairing stability.

In rare instances in mammals, miRNA–AGO2 cleaves target mRNA, creating unprotected 5′ and 3′ termini that are subject to endogenous RNase decay, thereby degrading the RNA (Shin et al., 2010; Yekta et al., 2004). More typically, miRNA–AGO does not function alone but rather recruits additional protein factors. After miRNA–AGO

binds to target RNA, TNRC6 binds to AGO (Fig. 3). TNRC6, GW182 in flies, is a ~182

kDa protein rich in glycine (G) and tryptophan (W); there are three TNRC6 paralogues

in humans, TNRC6A–C. The mammalian gene name *TNRC6* stands for trinucleotide-

repeat containing protein 6. TNRC6 was show to interact with AGO through reciprocal

co-IP experiments (Landthaler et al., 2008; Meister et al., 2005). The N-terminal half of

TNRC6 is the AGO-binding domain (ABD). It has three annotated AGO-binding

hotspots, is largely unstructured, and is rich in tryptophan residues (Pfaff et al., 2013).

Furthermore, TNRC6 has been shown to simultaneously interact with up to three AGO

proteins (Elkayam et al., 2017; Takimoto et al., 2009). AGO–TNRC6 interactions are

mediated via three W-binding pockets on the surface of AGO (Sheu-Gruttadauria and

MacRae, 2018).

The C-terminal half of TNRC6, termed the silencing domain, has motifs that

recruit factors responsible for the repression of mRNA targets (Braun et al., 2011;

Chekulaeva et al., 2011; Chen et al., 2014; Jonas and Izaurralde, 2015; Lazzaretti et al.,

2009). Through other tryptophan-mediated interactions, the silencing domain directly

interacts with PAN2/PAN3, which are non-processive deadenylases that shorten the

poly(A) tail of an mRNA (Christie et al., 2013). Via tryptophan-mediated binding

interactions in the silencing domain of TNRC6, NOT proteins are recruited to the

targeted mRNA. The CCR4/NOT complex has two deadenylases that shorten the

poly(A) tail (Basquin et al., 2012; Jonas and Izaurralde, 2015). NOT proteins also bind

DDX6, which represses translation (Chen et al., 2014; Kuzuoglu-Ozturk et al., 2016;

Mathys et al., 2014). Further protein-protein interactions recruit decapping enzymes,

including DCP2, which removes the 5′ m^{7}G cap from the mRNA, leaving the mRNA for

XRN1-mediated 5′-to-3′ degradation (Jonas and Izaurralde, 2015). Thus, miRNA-AGO

works to degrade an mRNA from both ends, first through deadenylation and then

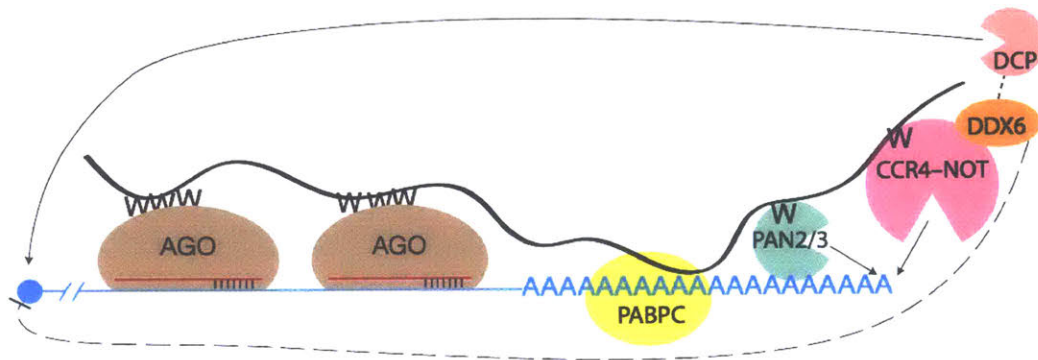through decapping (Chen et al., 2009).

Figure 3. miRNA-mediated target repression
miRNA–AGO (red and brown, respectively) bind mRNA (blue). TNRC6 (black) binds
miRNA–AGO through tryptophan-binding pockets on AGO and tryptophan residues (W)
on TNRC6. TNRC6 also binds PABPC (yellow) which is presumably already bound to
the mRNA poly(A) tail. TNRC6 recruits PAN2/PAN3 deadenylases (green) and CCR4–
NOT deadenylation complex (pink) which both deadenylate the mRNA. DDX6 (orange)
binds CCR4–NOT and translationally represses the mRNA. DCP (salmon) also interacts
with repressive machinery and decaps the mRNA. Decapped mRNA is subject to
XRN1-mediated 5′-to-3′ decay.

Inasmuch as miRNA–AGO–TNRC6 recruits factors for both translational

repression as well as deadenylation and decapping, studies have been carried out to

tease apart the contributions of each on posttranscriptional gene regulation. Ribosome

footprint profiling has been performed in combination with mRNA sequencing to assess

concomitant changes in transcript levels and translation. Initial studies in human and

mouse showed that miRNAs predominately downregulated gene expression via

degradation; translational repression accounted for ~11–16% of repression while mRNA

decay accounted for at least 84% of repression (Guo et al., 2010). In certain contexts,

such as early zebrafish development 4 h post-fertilization (hpf), translational repression

was found to be the dominant effect of miRNAs (Bazzini et al., 2012). Further

investigation into early developmental stages of zebrafish and frog revealed that

translational efficiency is coupled to poly(A)-tail length, but only for zebrafish up to 4 hpf,

and only for *Xenopus laevis* embryos up to stage 9 (Subtelny et al., 2014). The yeast,

mouse, and human samples examined failed to reveal any correlation between poly(A)-

tail length and translational efficiency (Subtelny et al., 2014). This correlation between

poly(A)-tail length and translational efficiency can be attributed to miRNAs shortening

poly(A)-tails and some feedback between tail length and translation. In zebrafish, after

the window of coupling between poly(A)-tail length and translational efficiency, i.e. at 6

hpf, miRNAs again predominantly act to decrease mRNA levels (Subtelny et al., 2014).

Examination of additional mammalian cell types and contexts found that miRNA-

mediated target degradation explained most of miRNA-mediated repression, and that if

translational repression occurs, by the time target is substantively repressed,

degradation is the main cause of repression (Eichhorn et al., 2014).

TNRC6

As discussed above, TNRC6 is a scaffold that recruits translational repression

and degradation machinery to target mRNAs. The C-terminal half of TNRC6 has

additional domains that do not interact with deadenylases, including an RNA-recognition

motif (RRM), poly(A)-binding protein (PABP)-interacting motif (PAM2 domain on

TNRC6), a glutamine (Q)-rich region, and a ubiquitin-associated (UBA) domain (Jonas and Izaurralde, 2015). Mutating the PAM2 domain of TNRC6 impedes the ability of miRNA–AGO–TNRC6 to repress targets (Huntzinger et al., 2013). The functions of the UBA and RRM have yet to be elucidated; mutating either domain has not been shown to alter target repression (Jonas and Izaurralde, 2015).

Both the N- and C-terminal halves of TNRC6 are necessary to elicit proper miRNA-mediated target silencing. The N-terminus binds AGO but the C-terminal silencing domain of TNRC6 cannot. However, if recombinant λN-fusion TNRC6 protein is tethered to the 3′ UTR of a reporter mRNA with BoxB sites, that mRNA will be repressed, as observed as a decrease in fluorescence reporter activity (Lazzaretti et al., 2009). Residues 599-683 of TNRC6B (AGO-APP) have been shown to strongly bind to human AGO2 (Hauptmann et al., 2015; Pfaff et al., 2013). If that peptide is expressed at high levels from a plasmid in HeLa cells, a global de-repression of target mRNAs is observed (Hauptmann et al., 2015). This de-repression occurs when AGO-APP outcompetes endogenous TNRC6. As AGO-APP does not have the silencing domain necessary for recruitment of repressive machinery, target mRNAs are no longer subject to miRNA-mediated repression.

TNRC6A has a nuclear export signal (NES) and a nuclear localization signal (NLS); TNRC6B and TNRC6C do not have an NLS (Nishi et al., 2013). Thus, while in mammals the action of miRNAs is largely in the cytoplasm, TNRC6A can be shuttled between the nucleus and cytoplasm. TNRC6 and AGO colocalize to cytoplasmic processing (P)-bodies. The Q-rich domain on TNRC6 has been shown to be necessary

for P-body localization in TNRC6B, but not TNRC6A (Lazzaretti et al., 2009). Deleting the Q-rich domain from TNRC6C has an intermediate effect, impairing by ~50% the localization of TNRC6C to P-bodies.

The interaction between TNRC6-ABD and AGO has been explored and found to be more nuanced than tryptophan–tryptophan-binding pocket. Binding of TNRC6 to AGO causes a structural change in AGO to close a gate around the tryptophan of TNRC6 to help secure the AGO–TNRC6 interaction (Elkayam et al., 2017). Although glycine residues often flank tryptophan residues in the ABD, neither the glycine nor other non-tryptophan residues on TNRC6 have been found to interact with AGO (Elkayam et al., 2017). Rather, in order to avoid steric clashes, the absence of bulky or aromatic side chains around the tryptophan enhances AGO–TNRC6 interactions (Pfaff et al., 2013). Each of the three tryptophan-binding pockets on the surface of AGO is ~25 Å from its two neighboring tryptophan-binding pockets (Sheu-Gruttadauria and MacRae, 2018). This three-dimensional distance corresponds to a flexible amino acid linker distance of 10-15 amino acid residues; indeed, tryptophan residues within the ABD of TNRC6 are spaced at a mean distance of 11.7 amino acids apart (Sheu-Gruttadauria and MacRae, 2018).

Further dissecting the interaction between individual binding pockets and TNRC6 proteins reveals a complex relationship. A 2016 study from the Izaurralde group, when only two tryptophan-binding pockets on AGO had been described, showed mutating one pocket on AGO had either very little effect (i.e. AGO2, pocket 1 mutant binds TNRC6B at almost native levels) or a very strong effect (i.e. AGO2, pocket 2 mutant has

extremely weak interaction with TNRC6C), depending on what pocket was mutated and which TNRC6 paralogue was binding (Kuzuoglu-Ozturk et al., 2016).

A 2018 study from the MacRae group, describing the three tryptophan-binding pockets on AGO2, investigated AGO–TNRC6B from both a TNRC6-centric and AGO2-centric approach. Different mutations in tryptophan residues of TNRC6B-ABD have a similarly complex relationship with AGO2 binding. Purified TNRC6B-ABD association with AGO2 was assessed with WT TNRC6B-ABD, and TNRC6B-ABD in which every tryptophan was mutated to an alanine (A). In the W to A mutant, no AGO2–TNRC6B-ABD interaction was observed (Sheu-Gruttadauria and MacRae, 2018). Restoring two W residues was sufficient to restore AGO–TNRC6B-ABD interaction. This restored interaction could again be ablated by mutating either of two tryptophan-binding pockets on the surface of AGO; mutating the third tryptophan-binding pocket does not impede AGO–TNRC6B-ABD (Sheu-Gruttadauria and MacRae, 2018). Alternatively, restoring three different W residues from A in a different stretch of TRNC6B-ABD was able to restore AGO–TRNC6B-ABD interactions with wild type AGO2. This TNRC6B-ABD peptide with three restored W residues was then tested for binding to each of the three AGO2 W pocket mutants; two pockets were found to be essential for binding and one pocket was found to be dispensable, but the dispensable pocket for these three W residues was different than the dispensable pocket for two different W residues (Sheu-Gruttadauria and MacRae, 2018). Thus, each tryptophan pocket on AGO2 has different binding preferences for different regions of TNRC6B-ABD. The root of these

preferences has not been explained by neighboring side chains or alternate AGO2–TNRC6 interactions.

Further nuances factor in to the affinities between AGO and TNRC6. The affinity of one AGO-binding hotspot, the "AGO hook" of TNRC6A (residues 821–841 of TNRC6A) was measured for binding AGO1 and for AGO2, each AGO either loaded or unloaded. Loaded AGO bound TNRC6 with ~5–8 times higher affinity than did unloaded AGO (Elkayam et al., 2017). A cellular benefit of a higher affinity for loaded AGO is that a loaded AGO engaged with target would better interact with TNRC6 and associated repressive machinery, leading to productive targeted degradation of an mRNA. An unloaded AGO-binding TNRC6 would not be able to direct repressive machinery to any specific target.

Additionally, although the N-terminal ABD of TNRC6 is thought of as largely unstructured, regulation of this region is possible. The affinity of any of the three AGO-binding hotspots alone at its tightest is 47 nM to AGO2 (Elkayam et al., 2017). However, the entire TNRC6A-ABD has an affinity of 7.7 nM for its first instance of binding to AGO2. The second AGO2 to bind the same molecule of TNRC6A-ABD does so at an affinity of 1 μM, despite the next tightest of the AGO hotspots having, in isolation, an affinity of 120 nM to AGO2 (Elkayam et al., 2017). Thus, binding of one AGO decreases the affinity of TNRC6 for subsequent AGO-binding. If an mRNA has two miRNA target sites spaced closely enough to bind the same TNRC6, binding the second AGO with decreased affinity may be biologically advantageous. If the first and second AGO-binding events had equal affinity, the cell may need to preload TNRC6 with the specific

23

miRNA–AGO complexes loaded with the specific miRNAs targeting the neighboring miRNA sites on a single target mRNA. Given the many different miRNA species expressed in one cell type at any given time, such prearrangement on TNRC6 would be statistically unlikely. Allowing miRNA–AGO to bind to target with pM affinity, and then recruit TNRC6, however, eliminates the need to preassemble specific miRNA–AGO on one TNRC6.

Although the above describes the mechanism of action of miRNA–AGO in the context of mammals, Argonaute was first described in plants as important for general plant architecture and leaf shape (Bohmert et al., 1998). In plants and yeast, AGO can work not only posttranscriptionally, but also on the chromatin level (Baulcombe, 2004; Verdel et al., 2004; Volpe et al., 2002). Argonaute proteins have been found across domains of life, from bacteria to mammals (Swarts et al., 2014b). The evolutionary origin of AGO is thought to be a defense mechanism against invading nucleic acid. Prokaryotic AGO can target mobile genetic elements as well as foreign DNA (Makarova et al., 2009; Olovnikov et al., 2013; Sheng et al., 2014; Swarts et al., 2014a). While eukaryotic AGOs use RNA guides to target RNA, prokaryotic AGOs can be loaded with DNA and/or RNA and can target DNA and/or RNA (Hegge et al., 2019; Swarts et al., 2015; Wang et al., 2008; Wang et al., 2009). *Thermus thermophilus* AGO decreases intracellular plasmid levels and plasmid transfection efficiency (Swarts et al., 2014a). The *C. elegans* genome encodes 27 Argonaute genes. *C. elegans* have a commensurate diversity of small RNAs with diverse targets and functions including gene regulation similar to that in mammals–worms produce miRNAs that act through

AIN-1 and AIN-2, which are TNRC6 orthologues–as well as small interfering RNAs (siRNAs) and secondary siRNAs generated via RNA-dependent RNA polymerases, which are found in plants and fungi but not mammals (Kuzuoglu-Ozturk et al., 2012; Yigit et al., 2006; Youngman and Claycomb, 2014). Overall, while AGO proteins are found throughout evolution, they have adapted varying means of regulating gene expression.

P-bodies and phase separation

Eukaryotic P-bodies are cytoplasmic foci enriched for mRNA decay factors (Decker and Parker, 2012). These foci are biomolecular condensates, or liquid-liquid phase-separated entities (Banani et al., 2017). Phase-separated liquid droplets are prone to occur through multivalent interactions between RNA and protein; intrinsically disordered regions (IRDs) also help promote phase separation (Banani et al., 2017; Lin et al., 2015). Phase separation occurs as a function of the solubility of macromolecules. If interactions between macromolecules and water are stronger than between macromolecules, molecules stay dissolved in water. However, if macromolecule–macromolecule interactions are stronger than those of macromolecule–water, phase separation will occur (Banani et al., 2017). Thus, many weak macromolecule–macromolecule interactions that may be mediated through the aforementioned multivalent interactions can contribute to phase separation.

Liquid-liquid phase-separated bodies have liquid like properties, including the ability to form droplets that can fuse with one another or bud off (Banani et al., 2017).

Phase-separated bodies are able, to varying extents, to exchange materials with their surroundings (Lin et al., 2015). Exchange with surroundings can be measured by fluorescence recovery after photobleaching (FRAP). A fluorescently labeled protein or RNA is mixed under the proper conditions to cause phase separation. Then, a laser is applied to photobleach the droplet and recovery of signal over time is measured. Exchange with surroundings may depend on the age of a droplet, as some droplets glassify over time and lose ability to exchange with surroundings (Lin et al., 2015).

Indeed, TNRC6 has properties typical of proteins that are prone to phase separation, including an IDR (the N-terminal ABD), RNA-binding (an RRM as well as AGO-mediated RNA binding), and multivalent interactions (binding multiple AGO proteins simultaneously). The properties of TNRC6B phase separation has been studied *in vitro* and *in vivo* (Sheu-Gruttadauria and MacRae, 2018). *In vitro*, purified human AGO2 was titrated into purified human TNRC6B-ABD and was shown to induce phase-separated bodies that included both TNRC6B-ABD and AGO2; these bodies were able to merge with one another over time. FRAP showed that these bodies exchanged both TNRC6B-ABD and AGO2 with surroundings, although AGO2 recovered more quickly and to a greater extent than TNRC6B-ABD (Sheu-Gruttadauria and MacRae, 2018).

Functional experiments by the MacRae group attempted to explore the idea that target mRNA deadenylation is enhanced in GW bodies. GW bodies were formed *in vitro* with 0.5 μM miRNA–AGO2, 1 μM TNRC6B, and soluble cellular lysate from HEK293 cells. Target RNA specifically bearing target sites to the miRNA with which AGO2 was

loaded was also sequestered by these droplets (Sheu-Gruttadauria and MacRae, 2018). AGO2 was active in these phase-separated bodies, as measured by its ability to cleave synthetic target RNA bearing a target site. Furthermore, components of the CCR4–NOT deadenylation complex, including CNOT7 and CNOT9, were present in these droplets whereas proteins present in cellular lysate but not part of miRNA-mediated target repression, such as Actin, were not in droplets (Sheu-Gruttadauria and MacRae, 2018).

To test if phase separation affects target deadenylation rates, miRNA–AGO2, TNRC6B, and cellular lysate were mixed at 200 nM miRNA–AGO2, 20 nM TNRC6B. However, at those relatively lower protein concentrations, droplets do not form. Thus, PEG8000 was added at 5% w/v to induce liquid-liquid phase separation (Sheu-Gruttadauria and MacRae, 2018). While synthetic target deadenylation was enhanced in these phase-separated droplets, PEG is a molecular crowding reagent which enhances reaction rates. Thus, under these conditions, it cannot be known whether or not increased target deadenylation was due to the generic crowding effects of PEG increasing reaction rate or to the enrichment of deadenylation machinery and activity in the phase-separated droplets.

TNRC6-phase-separation was also studied *in vivo*. GFP-tagged TNRC6B has been shown to form foci in human cells (Baillat and Shiekhattar, 2009; Sheu-Gruttadauria and MacRae, 2018). While these droplets can fuse with one another, they do not always merge after coming in contact, potentially indicating glassification (Sheu-Gruttadauria and MacRae, 2018). FRAP experiments of these bodies do show,

however, that these GW bodies are able to exchange contents with their surroundings (Sheu-Gruttadauria and MacRae, 2018). This study did not further examine the *in vivo* properties of miRNA-mediated target deadenylation in the context of TNRC6-mediated phase separation.

Although P-bodies were hypothesized to be sites of mRNA decay, knocking out various components required to microscopically visualize P-bodies does not necessarily impede mRNA decay (Luo et al., 2018). In an effort to use high-throughput techniques to characterize P-bodies, the Weil group developed a method called fluorescence-activated particle sorting (FAPS) to enrich P-bodies and subject them to mass spectroscopy and RNA-seq (Hubstenberger et al., 2017). A canonical P-body marker, LSM14A, was made as a transgene fused with GFP, and expressed in HEK293 cells. Cells were lysed, depleted of nuclei, and P-bodies were enriched by adapting a cell sorter to select GFP-positive particles on the size scale of P-bodies; a GFP-LSM14A mutant that does not localize to P-bodies was used as a negative control. Mass spec revealed an enrichment of proteins in P-bodies that are annotated to play a role in mRNA repression and decay, including DDX6, eIF4E-T, and AGO1, AGO2, and various DCP decapping enzymes. P-bodies were found to be translationally repressed and are depleted for ribosomes (Hubstenberger et al., 2017).

To investigate the decay status of mRNAs enriched in P-bodies, RNA-seq was performed on FAPS enriched particles and total mRNA. mRNAs depleted from P-bodies showed modestly decreased read density toward the 5′ end of the mRNA, relative to P-body enriched mRNAs. mRNAs enriched in P-bodies showed modestly decreased read

density toward the 3′ end. The authors suggest that the weakness of the signal indicates 3′ decay or 5′ protection are not enriched in P-bodies, but rather those characteristics might help induce a transcript to be shuttled to a P-body (Hubstenberger et al., 2017). However, during the P-body purification protocol, nucleases may remain active and degrade mRNAs with 5′-to-3′ decay pathways and that the degraded mRNA will then not appear in sequencing libraries.

A different investigation by the Chao group used single molecule imaging to assess mRNA decay in P-bodies. Using a reporter RNA with a 5′ end and 3′ end each separately visible in live-cell or fixed-cell imaging, the authors were able to visualize mRNA decay in P-bodies and cytoplasm. The 3′ end is protected from 5′-to-3′ decay by a pseudoknot resistant to Xrn1-mediated decay. They observed that, for this one reporter mRNA, mRNAs localized to P-bodies are not degraded, as evidenced by the fact that the 5′ and 3′ ends of the mRNAs colocalize in P-bodies; if P-bodies were sites of decay, the 3′ end would be expected to accumulate (Horvathova et al., 2017).

miRNAs targeting, regulation, and dysregulation

Since the initial characterization of a miRNA as a developmental regulator in *C. elegans*, the scope of miRNA and AGO biology has greatly expanded. Following the discovery of *lin-4* as a regulator of heterochronic genes, broad developmental roles of miRNAs have been described. In zebrafish, miR-430 is expressed at the start of zygotic transcription and functions in the maternal-to-zygotic transition (MZT) by aiding in the clearance of hundreds of maternally deposited mRNAs (Giraldez et al., 2006). In

contrast to the widespread effects of miR-430 in zebrafish MZT, in *C. elegans*, the

miRNA lsy-6 has been shown to function in the specification of one specific neuron

(Alberti and Cochella, 2017; Cochella and Hobert, 2012).

Hundreds of miRNAs have been identified in humans, flies, worms, and other

species (Bartel, 2018). Integral to understanding miRNA biology is knowing what

miRNAs are expressed, where, and when, and what specific mRNAs are targeted. Early

efforts to identify miRNA targeting showed that evolutionary conservation of miRNA

sites on mRNAs was sufficient to predict miRNA targets above false-positive rates

(Lewis et al., 2003). High-throughput sequencing of miRNAs has helped identify

expression and regulation patterns in time and space (de Rie et al., 2017; Landgraf et

al., 2007; Shenoy and Blelloch, 2014). In addition to identifying when miRNAs are

expressed, knowing which mRNAs miRNAs are actively targeting has been an area of

interest; various methods have been pioneered to attempt to identify specific

endogenous miRNA–AGO–target interactions. Such techniques often pair crosslinking

with high-throughput sequencing. For example, PAR-CLIP takes advantage of the

photoactivatable ribonucleoside 4-thiouridine (4SU), which can be incorporated into

RNAs by cellular polymerases and, upon exposure to 365 nm wavelength UV light,

crosslinks protein to RNA. After pulling down tagged AGO protein and sequencing, the

specific site of crosslinking can be identified (Hafner et al., 2010). Thus, one can pull on

AGO and see where exactly in the transcriptome it has bound. Interestingly, while

miRNAs predominantly act to target the 3′ UTR, 50% of crosslinked reads mapped to

CDS and 46% to 3′ UTR (Bartel, 2009; Hafner et al., 2010). However, those CDS sites

targeted by miRNAs were found to be only marginally effective. Similar techniques and analyses have attempted to identify miRNA-AGO–target interactions to assess target sites and pairing motifs (Broughton et al., 2016; Grosswendt et al., 2014; Helwak et al., 2013). Other large-scale efforts to predict miRNA targets have used data from a combination of miRNA transfections and miRNA knockouts to look, respectively, at downregulated and upregulated mRNAs (Agarwal et al., 2015; Grimson et al., 2007; Gumienny and Zavolan, 2015).

miRNA target prediction remains an open area of pursuit. The ever-expanding knowledge base on miRNAs simultaneously increases understanding while adding complexity. While in humans different miRNAs have not been shown to preferentially sort into different AGO paralogues, the miRNAs that are in different AGO proteins are of different lengths, with 3′ end differences likely due to tailing and trimming of the miRNA (Dueck et al., 2012). Furthermore, work from the Thompson lab showed that miRNA abundances do not always correlate with repression (La Rocca et al., 2015). In a survey of healthy adult mouse tissues, miRNA–Ago has been shown to be found in high molecular weight (HMW) complexes of >2 MDa, and in low molecular weight (LMW) complexes of ~100 kDa, as separated by size exclusion chromatography and visualized by Western blots against Ago2 (La Rocca et al., 2015). Some tissues, such as heart, skeletal muscle, and erythrocytes, only showed Ago2 in the LMW fraction. Brain, kidney, lymph nodes, and thymocytes showed Ago2 in both HMW and LMW fractions. Four of four cell lines showed Ago2 only in HMW fractions. RNase treatment showed that RNA-mediated interactions were necessary for migration at HWM; adding RNase

shifted Ago2 to an intermediate fraction size of ~500 kDa. TNRC6A–C also contributed to migration at HMW as siRNAs against TNRC6A–C shifted some of the HMW fraction to LMW.

T cell stimulation was then used to interrogate how miRNAs shift between LMW and HMW populations under different physiological conditions. Indeed, T cell stimulation caused miRNAs to redistribute between LMW and HMW. For tested miRNAs that redistributed to the HMW fraction but did not change expression levels, reporter assays showed that shifting to the HMW population increased ability of that miRNA to repress a reporter mRNA (La Rocca et al., 2015). These data point to the idea that some AGO is associated with TNRC6 and repressive machinery whereas other AGO is not, and that there may be cellular mechanisms for redistributing which expressed miRNAs are active under different cellular conditions.

An additional level of targeting regulation is the phosphorylation state of AGO. AGO has multiple annotated sites of phosphorylation; some sites affect AGO localization during stress conditions while other sites affect AGO targeting (Golden et al., 2017; Quevillon Huberdeau et al., 2017; Zeng et al., 2008). Five specific sites of phosphorylation on AGO were implicated in target binding; these residues are in the PIWI domain of AGO but are structurally unresolved. Serines and threonines are phosphorylated by the kinase CSNK1A1 while phosphatases ANKRD52 and PPP6C dephosphorylate the residues targeted by CSNK1A1. A phosphorylation cycle is established whereby the binding of miRNA–AGO to target triggers phosphorylation. Phosphorylation then decreases target binding; the residues that are phosphorylated

are near the miRNA–target interface (Golden et al., 2017). Furthermore, when AGO is phosphorylated, it binds to targets more selectively. Per eCLIP experiments, dephosphorylated AGO binds twice as many target sites as phosphorylated AGO. Dephosphorylated AGO binds the same repertoire of genes as phosphorylated AGO while also binding additional target genes. The authors posit that this forms a cycle of phosphorylation wherein dephosphorylated AGO binds to target. CSNK1A1 then phosphorylates AGO, which causes it to disengage from target, then ANKRD52/PPP6C dephosphorylates AGO such that it can reengage another target. Disruption of this cycle globally impairs miRNA-mediated target repression (Golden et al., 2017).

Given the impact miRNAs can have on normal cellular functions, it is unsurprising that miRNAs can be dysregulated in disease, in both functional ways and as biomarkers for disease state (Cullen, 2013; Lai et al., 2015; Max et al., 2018; Renwick et al., 2013; Wang et al., 2016). For example, the *Herpesvirus saimiri* (HVS) transcript HSUR1 has target sites for miR-27 that cause the miRNA to be degraded and the targets of miR-27 to increase in abundance (Cazalla et al., 2010). The *Herpesvirus saimiri* transcript HSUR2 employs a unique mechanism of regulating host mRNA levels. HSUR2 has a target site for each of miR-16 and miR-142-3p. Also, as identified through psoralen-mediated crosslinking and sequencing experiments, HSUR2 base-pairs to a subset of cellular mRNAs (Gorbea et al., 2017). The effect of this base pairing is to tether the miRNA–AGO to HSUR2-bound mRNA, leading to the downregulation of HSUR2-bound mRNAs. mRNAs bound by HSUR2 were enriched for genes involved in p53 signaling. Overall, HSUR2 works to decrease cellular apoptosis of infected cells as

compared to cells infected with HVS that lacks HSUR2 (Gorbea et al., 2017). Whereas

AGO proteins and RNAi are thought to have evolved as a host defense against invading

nucleic acids, the evolutionary arms race has progressed such that virus is now

hijacking AGO to abet cellular infection.

This thesis focuses on an additional aspect of miRNA targeting and efficacy: the

cooperative action of closely spaced miRNA binding events (Grimson et al., 2007;

Saetrom et al., 2007). When two miRNAs target the same transcript and the binding

sites for those sites are < 40 and > 7 nt apart (counting between the 3′ end of the

upstream site and the 5′ end of the downstream site), those two sites act synergistically

to repress the mRNA more than expected if the two sites were to act independently

(Grimson et al., 2007). Previous studies have phenomenologically investigated

parameters for cooperatively *in vivo* using mRNA reporter assays (Broderick et al.,

2011; Doench et al., 2003). This dissertation uses purified components and *in vitro*

assays to biochemically dissect the molecular factors responsible for cooperative

repression of mRNAs with closely spaced miRNA target sites.

References

Agarwal, V., Bell, G.W., Nam, J.W., and Bartel, D.P. (2015). Predicting effective microRNA target sites in mammalian mRNAs. eLife *4*.

Alberti, C., and Cochella, L. (2017). A framework for understanding the roles of miRNAs in animal development. Development *144*, 2548-2559.

Baillat, D., and Shiekhattar, R. (2009). Functional dissection of the human TNRC6 (GW182-related) family of proteins. Mol Cell Biol *29*, 4144-4155.

Banani, S.F., Lee, H.O., Hyman, A.A., and Rosen, M.K. (2017). Biomolecular condensates: organizers of cellular biochemistry. Nat Rev Mol Cell Biol *18*, 285-298.

Bartel, D.P. (2004). MicroRNAs. Cell *116*, 281-297.

Bartel, D.P. (2009). MicroRNAs: target recognition and regulatory functions. Cell *136*, 215-233.

Bartel, D.P. (2018). Metazoan MicroRNAs. Cell *173*, 20-51.

Basquin, J., Roudko, V.V., Rode, M., Basquin, C., Seraphin, B., and Conti, E. (2012). Architecture of the nuclease module of the yeast Ccr4-not complex: the Not1-Caf1-Ccr4 interaction. Molecular cell *48*, 207-218.

Baulcombe, D. (2004). RNA silencing in plants. Nature *431*, 356-363.

Bazzini, A.A., Lee, M.T., and Giraldez, A.J. (2012). Ribosome profiling shows that miR-430 reduces translation before causing mRNA decay in zebrafish. Science *336*, 233-237.

Bernstein, E., Caudy, A.A., Hammond, S.M., and Hannon, G.J. (2001). Role for a bidentate ribonuclease in the initiation step of RNA interference. Nature *409*, 363-366.

Bohmert, K., Camus, I., Bellini, C., Bouchez, D., Caboche, M., and Benning, C. (1998). AGO1 defines a novel locus of Arabidopsis controlling leaf development. The EMBO journal *17*, 170-180.

Braun, J.E., Huntzinger, E., Fauser, M., and Izaurralde, E. (2011). GW182 proteins directly recruit cytoplasmic deadenylase complexes to miRNA targets. Molecular cell *44*, 120-133.

Brennecke, J., Stark, A., Russell, R.B., and Cohen, S.M. (2005). Principles of microRNA-target recognition. PLoS Biol *3*, e85.

Broderick, J.A., Salomon, W.E., Ryder, S.P., Aronin, N., and Zamore, P.D. (2011). Argonaute protein identity and pairing geometry determine cooperativity in mammalian RNA silencing. Rna *17*, 1858-1869.

Broughton, J.P., Lovci, M.T., Huang, J.L., Yeo, G.W., and Pasquinelli, A.E. (2016). Pairing beyond the Seed Supports MicroRNA Targeting Specificity. Molecular cell *64*, 320-333.

Cai, X., Hagedorn, C.H., and Cullen, B.R. (2004). Human microRNAs are processed from capped, polyadenylated transcripts that can also function as mRNAs. Rna *10*, 1957-1966.

Cazalla, D., Yario, T., and Steitz, J.A. (2010). Down-regulation of a host microRNA by a Herpesvirus saimiri noncoding RNA. Science *328*, 1563-1566.

Chandradoss, S.D., Schirle, N.T., Szczepaniak, M., MacRae, I.J., and Joo, C. (2015). A Dynamic Search Process Underlies MicroRNA Targeting. Cell *162*, 96-107.

Chekulaeva, M., Mathys, H., Zipprich, J.T., Attig, J., Colic, M., Parker, R., and Filipowicz, W. (2011). miRNA repression involves GW182-mediated recruitment of CCR4-NOT through conserved W-containing motifs. Nature structural & molecular biology *18*, 1218-1226.

Cheloufi, S., Dos Santos, C.O., Chong, M.M., and Hannon, G.J. (2010). A dicer-independent miRNA biogenesis pathway that requires Ago catalysis. Nature *465*, 584-589.

Chen, C.Y., Zheng, D., Xia, Z., and Shyu, A.B. (2009). Ago-TNRC6 triggers microRNA-mediated decay by promoting two deadenylation steps. Nature structural & molecular biology *16*, 1160-1166.

Chen, Y., Boland, A., Kuzuoglu-Ozturk, D., Bawankar, P., Loh, B., Chang, C.T., Weichenrieder, O., and Izaurralde, E. (2014). A DDX6-CNOT1 complex and W-binding pockets in CNOT9 reveal direct links between miRNA target recognition and silencing. Molecular cell *54*, 737-750.

Christie, M., Boland, A., Huntzinger, E., Weichenrieder, O., and Izaurralde, E. (2013). Structure of the PAN3 pseudokinase reveals the basis for interactions with the PAN2 deadenylase and the GW182 proteins. Molecular cell *51*, 360-373.

Cifuentes, D., Xue, H., Taylor, D.W., Patnode, H., Mishima, Y., Cheloufi, S., Ma, E., Mane, S., Hannon, G.J., Lawson, N.D.*, et al.* (2010). A novel miRNA processing pathway independent of Dicer requires Argonaute2 catalytic activity. Science *328*, 1694-1698.

Cochella, L., and Hobert, O. (2012). Embryonic priming of a miRNA locus predetermines postmitotic neuronal left/right asymmetry in C. elegans. Cell *151*, 1229-1242.

Cullen, B.R. (2013). MicroRNAs as mediators of viral evasion of the immune system. Nature immunology *14*, 205-210.

de Rie, D., Abugessaisa, I., Alam, T., Arner, E., Arner, P., Ashoor, H., Astrom, G., Babina, M., Bertin, N., Burroughs, A.M.*, et al.* (2017). An integrated expression atlas of miRNAs and their promoters in human and mouse. Nature biotechnology *35*, 872-878.

Decker, C.J., and Parker, R. (2012). P-bodies and stress granules: possible roles in the control of translation and mRNA degradation. Cold Spring Harb Perspect Biol *4*, a012286.

Doench, J.G., Petersen, C.P., and Sharp, P.A. (2003). siRNAs can function as miRNAs. Genes & development *17*, 438-442.

Doench, J.G., and Sharp, P.A. (2004). Specificity of microRNA target selection in translational repression. Genes & development *18*, 504-511.

Dueck, A., Ziegler, C., Eichner, A., Berezikov, E., and Meister, G. (2012). microRNAs associated with the different human Argonaute proteins. Nucleic acids research *40*, 9850-9862.

Eichhorn, S.W., Guo, H., McGeary, S.E., Rodriguez-Mias, R.A., Shin, C., Baek, D., Hsu, S.H., Ghoshal, K., Villen, J., and Bartel, D.P. (2014). mRNA destabilization is the

dominant effect of mammalian microRNAs by the time substantial repression ensues. Molecular cell *56*, 104-115.

Elbashir, S.M., Lendeckel, W., and Tuschl, T. (2001). RNA interference is mediated by 21- and 22-nucleotide RNAs. Genes & development *15*, 188-200.

Elkayam, E., Faehnle, C.R., Morales, M., Sun, J., Li, H., and Joshua-Tor, L. (2017). Multivalent Recruitment of Human Argonaute by GW182. Molecular cell *67*, 646-658 e643.

Elkayam, E., Kuhn, C.D., Tocilj, A., Haase, A.D., Greene, E.M., Hannon, G.J., and Joshua-Tor, L. (2012). The structure of human argonaute-2 in complex with miR-20a. Cell *150*, 100-110.

Faehnle, C.R., Elkayam, E., Haase, A.D., Hannon, G.J., and Joshua-Tor, L. (2013). The making of a slicer: activation of human Argonaute-1. Cell reports *3*, 1901-1909.

Fang, W., and Bartel, D.P. (2015). The Menu of Features that Define Primary MicroRNAs and Enable De Novo Design of MicroRNA Genes. Molecular cell *60*, 131-145.

Friedman, R.C., Farh, K.K., Burge, C.B., and Bartel, D.P. (2009). Most mammalian mRNAs are conserved targets of microRNAs. Genome research *19*, 92-105.

Giraldez, A.J., Mishima, Y., Rihel, J., Grocock, R.J., Van Dongen, S., Inoue, K., Enright, A.J., and Schier, A.F. (2006). Zebrafish MiR-430 promotes deadenylation and clearance of maternal mRNAs. Science *312*, 75-79.

Golden, R.J., Chen, B., Li, T., Braun, J., Manjunath, H., Chen, X., Wu, J., Schmid, V., Chang, T.C., Kopp, F., *et al.* (2017). An Argonaute phosphorylation cycle promotes microRNA-mediated silencing. Nature *542*, 197-202.

Gorbea, C., Mosbruger, T., and Cazalla, D. (2017). A viral Sm-class RNA base-pairs with mRNAs and recruits microRNAs to inhibit apoptosis. Nature *550*, 275-279.

Grimson, A., Farh, K.K., Johnston, W.K., Garrett-Engele, P., Lim, L.P., and Bartel, D.P. (2007). MicroRNA targeting specificity in mammals: determinants beyond seed pairing. Molecular cell *27*, 91-105.

Grosswendt, S., Filipchyk, A., Manzano, M., Klironomos, F., Schilling, M., Herzog, M., Gottwein, E., and Rajewsky, N. (2014). Unambiguous identification of miRNA:target site interactions by different types of ligation reactions. Molecular cell *54*, 1042-1054.

Gumienny, R., and Zavolan, M. (2015). Accurate transcriptome-wide prediction of microRNA targets and small interfering RNA off-targets with MIRZA-G. Nucleic acids research *43*, 1380-1391.

Guo, H., Ingolia, N.T., Weissman, J.S., and Bartel, D.P. (2010). Mammalian microRNAs predominantly act to decrease target mRNA levels. Nature *466*, 835-840.

Ha, M., and Kim, V.N. (2014). Regulation of microRNA biogenesis. Nat Rev Mol Cell Biol *15*, 509-524.

Hafner, M., Landthaler, M., Burger, L., Khorshid, M., Hausser, J., Berninger, P., Rothballer, A., Ascano, M., Jr., Jungkamp, A.C., Munschauer, M., *et al.* (2010). Transcriptome-wide identification of RNA-binding protein and microRNA target sites by PAR-CLIP. Cell *141*, 129-141.

Han, J., Lee, Y., Yeom, K.H., Kim, Y.K., Jin, H., and Kim, V.N. (2004). The Drosha-DGCR8 complex in primary microRNA processing. Genes & development *18*, 3016-3027.

Hauptmann, J., Dueck, A., Harlander, S., Pfaff, J., Merkl, R., and Meister, G. (2013). Turning catalytically inactive human Argonaute proteins into active slicer enzymes. Nature structural & molecular biology *20*, 814-817.

Hauptmann, J., Schraivogel, D., Bruckmann, A., Manickavel, S., Jakob, L., Eichner, N., Pfaff, J., Urban, M., Sprunck, S., Hafner, M., *et al.* (2015). Biochemical isolation of Argonaute protein complexes by Ago-APP. Proceedings of the National Academy of Sciences of the United States of America *112*, 11841-11845.

Hegge, J.W., Swarts, D.C., Chandradoss, S.D., Cui, T.J., Kneppers, J., Jinek, M., Joo, C., and van der Oost, J. (2019). DNA-guided DNA cleavage at moderate temperatures by Clostridium butyricum Argonaute. Nucleic acids research *47*, 5809-5821.

Helwak, A., Kudla, G., Dudnakova, T., and Tollervey, D. (2013). Mapping the human miRNA interactome by CLASH reveals frequent noncanonical binding. Cell *153*, 654-665.

Horvathova, I., Voigt, F., Kotrys, A.V., Zhan, Y., Artus-Revel, C.G., Eglinger, J., Stadler, M.B., Giorgetti, L., and Chao, J.A. (2017). The Dynamics of mRNA Turnover Revealed by Single-Molecule Imaging in Single Cells. Molecular cell *68*, 615-625 e619.

Hubstenberger, A., Courel, M., Benard, M., Souquere, S., Ernoult-Lange, M., Chouaib, R., Yi, Z., Morlot, J.B., Munier, A., Fradet, M., *et al.* (2017). P-Body Purification Reveals the Condensation of Repressed mRNA Regulons. Molecular cell *68*, 144-157 e145.

Huntzinger, E., Kuzuoglu-Ozturk, D., Braun, J.E., Eulalio, A., Wohlbold, L., and Izaurralde, E. (2013). The interactions of GW182 proteins with PABP and deadenylases are required for both translational repression and degradation of miRNA targets. Nucleic acids research *41*, 978-994.

Hutvagner, G., McLachlan, J., Pasquinelli, A.E., Balint, E., Tuschl, T., and Zamore, P.D. (2001). A cellular function for the RNA-interference enzyme Dicer in the maturation of the let-7 small temporal RNA. Science *293*, 834-838.

Jee, D., Yang, J.S., Park, S.M., Farmer, D.T., Wen, J., Chou, T., Chow, A., McManus, M.T., Kharas, M.G., and Lai, E.C. (2018). Dual Strategies for Argonaute2-Mediated Biogenesis of Erythroid miRNAs Underlie Conserved Requirements for Slicing in Mammals. Molecular cell *69*, 265-278 e266.

Jonas, S., and Izaurralde, E. (2015). Towards a molecular understanding of microRNA-mediated gene silencing. Nature reviews Genetics *16*, 421-433.

Khvorova, A., Reynolds, A., and Jayasena, S.D. (2003). Functional siRNAs and miRNAs Exhibit Strand Bias. Cell *115*, 209-216.

Kuzuoglu-Ozturk, D., Bhandari, D., Huntzinger, E., Fauser, M., Helms, S., and Izaurralde, E. (2016). miRISC and the CCR4-NOT complex silence mRNA targets independently of 43S ribosomal scanning. The EMBO journal.

Kuzuoglu-Ozturk, D., Huntzinger, E., Schmidt, S., and Izaurralde, E. (2012). The Caenorhabditis elegans GW182 protein AIN-1 interacts with PAB-1 and subunits of the PAN2-PAN3 and CCR4-NOT deadenylase complexes. Nucleic acids research *40*, 5651-5665.

Kwon, S.C., Nguyen, T.A., Choi, Y.G., Jo, M.H., Hohng, S., Kim, V.N., and Woo, J.S. (2016). Structure of Human DROSHA. Cell *164*, 81-90.

La Rocca, G., Olejniczak, S.H., Gonzalez, A.J., Briskin, D., Vidigal, J.A., Spraggon, L., DeMatteo, R.G., Radler, M.R., Lindsten, T., Ventura, A., *et al.* (2015). In vivo, Argonaute-bound microRNAs exist predominantly in a reservoir of low molecular weight complexes not associated with mRNA. Proceedings of the National Academy of Sciences of the United States of America *112*, 767-772.

Lagos-Quintana, M., Rauhut, R., Lendeckel, W., and Tuschl, T. (2001). Identification of novel genes coding for small expressed RNAs. Science *294*, 853-858.

Lai, J.Y., Luo, J., O'Connor, C., Jing, X., Nair, V., Ju, W., Randolph, A., Ben-Dov, I.Z., Matar, R.N., Briskin, D., *et al.* (2015). MicroRNA-21 in glomerular injury. Journal of the American Society of Nephrology : JASN *26*, 805-816.

Landgraf, P., Rusu, M., Sheridan, R., Sewer, A., Iovino, N., Aravin, A., Pfeffer, S., Rice, A., Kamphorst, A.O., Landthaler, M., *et al.* (2007). A mammalian microRNA expression atlas based on small RNA library sequencing. Cell *129*, 1401-1414.

Landthaler, M., Gaidatzis, D., Rothballer, A., Chen, P.Y., Soll, S.J., Dinic, L., Ojo, T., Hafner, M., Zavolan, M., and Tuschl, T. (2008). Molecular characterization of human Argonaute-containing ribonucleoprotein complexes and their bound target mRNAs. Rna *14*, 2580-2596.

Lazzaretti, D., Tournier, I., and Izaurralde, E. (2009). The C-terminal domains of human TNRC6A, TNRC6B, and TNRC6C silence bound transcripts independently of Argonaute proteins. Rna *15*, 1059-1066.

Lee, R.C., Feinbaum, R.L., and Ambros, V. (1993). The C. elegans heterochronic gene lin-4 encodes small RNAs with antisense complementarity to lin-14. Cell *75*, 843-854.

Lee, Y., Kim, M., Han, J., Yeom, K.H., Lee, S., Baek, S.H., and Kim, V.N. (2004). MicroRNA genes are transcribed by RNA polymerase II. The EMBO journal *23*, 4051-4060.

Lewis, B.P., Burge, C.B., and Bartel, D.P. (2005). Conserved seed pairing, often flanked by adenosines, indicates that thousands of human genes are microRNA targets. Cell *120*, 15-20.

Lewis, B.P., Shih, I.H., Jones-Rhoades, M.W., Bartel, D.P., and Burge, C.B. (2003). Prediction of mammalian microRNA targets. Cell *115*, 787-798.

Lin, Y., Protter, D.S., Rosen, M.K., and Parker, R. (2015). Formation and Maturation of Phase-Separated Liquid Droplets by RNA-Binding Proteins. Molecular cell *60*, 208-219.

Liu, J., Carmell, M.A., Rivas, F.V., Marsden, C.G., Thomson, J.M., Song, J.J., Hammond, S.M., Joshua-Tor, L., and Hannon, G.J. (2004). Argonaute2 is the catalytic engine of mammalian RNAi. Science *305*, 1437-1441.

Lund, E., Guttinger, S., Calado, A., Dahlberg, J.E., and Kutay, U. (2004). Nuclear export of microRNA precursors. Science *303*, 95-98.

Luo, Y., Na, Z., and Slavoff, S.A. (2018). P-Bodies: Composition, Properties, and Functions. Biochemistry *57*, 2424-2431.

Ma, J.B., Yuan, Y.R., Meister, G., Pei, Y., Tuschl, T., and Patel, D.J. (2005). Structural basis for 5'-end-specific recognition of guide RNA by the A. fulgidus Piwi protein. Nature *434*, 666-670.

Makarova, K.S., Wolf, Y.I., van der Oost, J., and Koonin, E.V. (2009). Prokaryotic homologs of Argonaute proteins are predicted to function as key components of a novel system of defense against mobile genetic elements. Biol Direct *4*, 29.

Mathys, H., Basquin, J., Ozgur, S., Czarnocki-Cieciura, M., Bonneau, F., Aartse, A., Dziembowski, A., Nowotny, M., Conti, E., and Filipowicz, W. (2014). Structural and biochemical insights to the role of the CCR4-NOT complex and DDX6 ATPase in microRNA repression. Molecular cell *54*, 751-765.

Max, K.E.A., Bertram, K., Akat, K.M., Bogardus, K.A., Li, J., Morozov, P., Ben-Dov, I.Z., Li, X., Weiss, Z.R., Azizian, A., *et al.* (2018). Human plasma and serum extracellular small RNA reference profiles and their clinical utility. Proceedings of the National Academy of Sciences of the United States of America *115*, E5334-E5343.

Meister, G., Landthaler, M., Patkaniowska, A., Dorsett, Y., Teng, G., and Tuschl, T. (2004). Human Argonaute2 mediates RNA cleavage targeted by miRNAs and siRNAs. Molecular cell *15*, 185-197.

Meister, G., Landthaler, M., Peters, L., Chen, P.Y., Urlaub, H., Luhrmann, R., and Tuschl, T. (2005). Identification of novel argonaute-associated proteins. Curr Biol *15*, 2149-2155.

Nakanishi, K., Ascano, M., Gogakos, T., Ishibe-Murakami, S., Serganov, A.A., Briskin, D., Morozov, P., Tuschl, T., and Patel, D.J. (2013). Eukaryote-specific insertion elements control human ARGONAUTE slicer activity. Cell reports *3*, 1893-1900.

Nakanishi, K., Weinberg, D.E., Bartel, D.P., and Patel, D.J. (2012). Structure of yeast Argonaute with guide RNA. Nature *486*, 368-374.

Nishi, K., Nishi, A., Nagasawa, T., and Ui-Tei, K. (2013). Human TNRC6A is an Argonaute-navigator protein for microRNA-mediated gene silencing in the nucleus. Rna *19*, 17-35.

Olovnikov, I., Chan, K., Sachidanandam, R., Newman, D.K., and Aravin, A.A. (2013). Bacterial argonaute samples the transcriptome to identify foreign DNA. Molecular cell *51*, 594-605.

Park, J.E., Heo, I., Tian, Y., Simanshu, D.K., Chang, H., Jee, D., Patel, D.J., and Kim, V.N. (2011). Dicer recognizes the 5' end of RNA for efficient and accurate processing. Nature *475*, 201-205.

Park, M.S., Araya-Secchi, R., Brackbill, J.A., Phan, H.D., Kehling, A.C., Abd El-Wahab, E.W., Dayeh, D.M., Sotomayor, M., and Nakanishi, K. (2019). Multidomain Convergence of Argonaute during RISC Assembly Correlates with the Formation of Internal Water Clusters. Molecular cell.

Park, M.S., Phan, H.D., Busch, F., Hinckley, S.H., Brackbill, J.A., Wysocki, V.H., and Nakanishi, K. (2017). Human Argonaute3 has slicer activity. Nucleic acids research *45*, 11867-11877.

Parker, J.S., Roe, S.M., and Barford, D. (2005). Structural insights into mRNA recognition from a PIWI domain-siRNA guide complex. Nature *434*, 663-666.

Pfaff, J., Hennig, J., Herzog, F., Aebersold, R., Sattler, M., Niessing, D., and Meister, G. (2013). Structural features of Argonaute-GW182 protein interactions. Proceedings of the National Academy of Sciences of the United States of America *110*, E3770-3779.

Quevillon Huberdeau, M., Zeitler, D.M., Hauptmann, J., Bruckmann, A., Fressigne, L., Danner, J., Piquet, S., Strieder, N., Engelmann, J.C., Jannot, G., *et al.* (2017). Phosphorylation of Argonaute proteins affects mRNA binding and is essential for microRNA-guided gene silencing in vivo. The EMBO journal *36*, 2088-2106.

Renwick, N., Cekan, P., Masry, P.A., McGeary, S.E., Miller, J.B., Hafner, M., Li, Z., Mihailovic, A., Morozov, P., Brown, M., *et al.* (2013). Multicolor microRNA FISH effectively differentiates tumor types. The Journal of clinical investigation *123*, 2694-2702.

Saetrom, P., Heale, B.S., Snove, O., Jr., Aagaard, L., Alluin, J., and Rossi, J.J. (2007). Distance constraints between microRNA target sites dictate efficacy and cooperativity. Nucleic acids research *35*, 2333-2342.

Salomon, W.E., Jolly, S.M., Moore, M.J., Zamore, P.D., and Serebrov, V. (2015). Single-Molecule Imaging Reveals that Argonaute Reshapes the Binding Properties of Its Nucleic Acid Guides. Cell *162*, 84-95.

Schirle, N.T., and MacRae, I.J. (2012). The crystal structure of human Argonaute2. Science *336*, 1037-1040.

Schirle, N.T., Sheu-Gruttadauria, J., Chandradoss, S.D., Joo, C., and MacRae, I.J. (2015). Water-mediated recognition of t1-adenosine anchors Argonaute2 to microRNA targets. eLife *4*.

Schirle, N.T., Sheu-Gruttadauria, J., and MacRae, I.J. (2014). Structural basis for microRNA targeting. Science *346*, 608-613.

Schwarz, D.S., Hutvágner, G., Du, T., Xu, Z., Aronin, N., and Zamore, P.D. (2003). Asymmetry in the Assembly of the RNAi Enzyme Complex. Cell *115*, 199-208.

Sheng, G., Zhao, H., Wang, J., Rao, Y., Tian, W., Swarts, D.C., van der Oost, J., Patel, D.J., and Wang, Y. (2014). Structure-based cleavage mechanism of Thermus thermophilus Argonaute DNA guide strand-mediated DNA target cleavage. Proceedings of the National Academy of Sciences of the United States of America *111*, 652-657.

Shenoy, A., and Blelloch, R.H. (2014). Regulation of microRNA function in somatic stem cell proliferation and differentiation. Nat Rev Mol Cell Biol *15*, 565-576.

Sheu-Gruttadauria, J., and MacRae, I.J. (2018). Phase Transitions in the Assembly and Function of Human miRISC. Cell *173*, 946-957 e916.

Sheu-Gruttadauria, J., Xiao, Y., Gebert, L.F.R., and MacRae, I.J. (2019). Beyond the seed: structural basis for supplementary microRNA targeting by human Argonaute2. The EMBO journal.

Shin, C., Nam, J.W., Farh, K.K., Chiang, H.R., Shkumatava, A., and Bartel, D.P. (2010). Expanding the microRNA targeting code: functional sites with centered pairing. Molecular cell *38*, 789-802.

Siolas, D., Lerner, C., Burchard, J., Ge, W., Linsley, P.S., Paddison, P.J., Hannon, G.J., and Cleary, M.A. (2005). Synthetic shRNAs as potent RNAi triggers. Nature biotechnology *23*, 227-231.

Song, J.J., Smith, S.K., Hannon, G.J., and Joshua-Tor, L. (2004). Crystal structure of Argonaute and its implications for RISC slicer activity. Science *305*, 1434-1437.

Subtelny, A.O., Eichhorn, S.W., Chen, G.R., Sive, H., and Bartel, D.P. (2014). Poly(A)-tail profiling reveals an embryonic switch in translational control. Nature *508*, 66-71.

Suzuki, H.I., Katsura, A., Yasuda, T., Ueno, T., Mano, H., Sugimoto, K., and Miyazono, K. (2015). Small-RNA asymmetry is directly driven by mammalian Argonautes. Nature structural & molecular biology *22*, 512-521.

Swarts, D.C., Hegge, J.W., Hinojo, I., Shiimori, M., Ellis, M.A., Dumrongkulraksa, J., Terns, R.M., Terns, M.P., and van der Oost, J. (2015). Argonaute of the archaeon Pyrococcus furiosus is a DNA-guided nuclease that targets cognate DNA. Nucleic acids research *43*, 5120-5129.

Swarts, D.C., Jore, M.M., Westra, E.R., Zhu, Y., Janssen, J.H., Snijders, A.P., Wang, Y., Patel, D.J., Berenguer, J., Brouns, S.J., *et al.* (2014a). DNA-guided DNA interference by a prokaryotic Argonaute. Nature *507*, 258-261.

Swarts, D.C., Makarova, K., Wang, Y., Nakanishi, K., Ketting, R.F., Koonin, E.V., Patel, D.J., and van der Oost, J. (2014b). The evolutionary journey of Argonaute proteins. Nature structural & molecular biology *21*, 743-753.

Takimoto, K., Wakiyama, M., and Yokoyama, S. (2009). Mammalian GW182 contains multiple Argonaute-binding sites and functions in microRNA-mediated translational repression. Rna *15*, 1078-1089.

Tian, Y., Simanshu, D.K., Ma, J.B., Park, J.E., Heo, I., Kim, V.N., and Patel, D.J. (2014). A phosphate-binding pocket within the platform-PAZ-connector helix cassette of human Dicer. Molecular cell *53*, 606-616.

Verdel, A., Jia, S., Gerber, S., Sugiyama, T., Gygi, S., Grewal, S.I., and Moazed, D. (2004). RNAi-mediated targeting of heterochromatin by the RITS complex. Science *303*, 672-676.

Volpe, T.A., Kidner, C., Hall, I.M., Teng, G., Grewal, S.I., and Martienssen, R.A. (2002). Regulation of heterochromatic silencing and histone H3 lysine-9 methylation by RNAi. Science *297*, 1833-1837.

Wang, J., Chen, J., and Sen, S. (2016). MicroRNA as Biomarkers and Diagnostics. J Cell Physiol *231*, 25-30.

Wang, Y., Juranek, S., Li, H., Sheng, G., Tuschl, T., and Patel, D.J. (2008). Structure of an argonaute silencing complex with a seed-containing guide DNA and target RNA duplex. Nature *456*, 921-926.

Wang, Y., Juranek, S., Li, H., Sheng, G., Wardle, G.S., Tuschl, T., and Patel, D.J. (2009). Nucleation, propagation and cleavage of target RNAs in Ago silencing complexes. Nature *461*, 754-761.

Wee, L.M., Flores-Jasso, C.F., Salomon, W.E., and Zamore, P.D. (2012). Argonaute divides its RNA guide into domains with distinct functions and RNA-binding properties. Cell *151*, 1055-1067.

Wightman, B., Ha, I., and Ruvkun, G. (1993). Posttranscriptional regulation of the heterochronic gene lin-14 by lin-4 mediates temporal pattern formation in C. elegans. Cell *75*, 855-862.

Yekta, S., Shih, I.H., and Bartel, D.P. (2004). MicroRNA-directed cleavage of HOXB8 mRNA. Science *304*, 594-596.

Yi, R., Qin, Y., Macara, I.G., and Cullen, B.R. (2003). Exportin-5 mediates the nuclear export of pre-microRNAs and short hairpin RNAs. Genes & development *17*, 3011-3016.

Yigit, E., Batista, P.J., Bei, Y., Pang, K.M., Chen, C.C., Tolia, N.H., Joshua-Tor, L., Mitani, S., Simard, M.J., and Mello, C.C. (2006). Analysis of the C. elegans Argonaute family reveals that distinct Argonautes act sequentially during RNAi. Cell *127*, 747-757.

Yoda, M., Cifuentes, D., Izumi, N., Sakaguchi, Y., Suzuki, T., Giraldez, A.J., and Tomari, Y. (2013). Poly(A)-specific ribonuclease mediates 3'-end trimming of Argonaute2-cleaved precursor microRNAs. Cell reports *5*, 715-726.

Youngman, E.M., and Claycomb, J.M. (2014). From early lessons to new frontiers: the worm as a treasure trove of small RNA biology. Frontiers in genetics *5*, 416.

Zeng, Y., Sankala, H., Zhang, X., and Graves, P.R. (2008). Phosphorylation of Argonaute 2 at serine-387 facilitates its localization to processing bodies. Biochem J *413*, 429-436.

Zhang, H., Kolb, F.A., Brondani, V., Billy, E., and Filipowicz, W. (2002). Human Dicer preferentially cleaves dsRNAs at their termini without a requirement for ATP. The EMBO journal *21*, 5875-5885.

Chapter 2. The biochemical basis for the cooperative action of microRNAs

Daniel Briskin[a,b,c], David P. Bartel[a,b,c]

[a]Whitehead Institute for Biomedical Research, 455 Main Street, Cambridge, MA, 02142; [b]Howard Hughes Medical Institute, Cambridge, MA, 02142; and [c]Department of Biology, Massachusetts Institute of Technology, Cambridge, MA, 02139

Abstract

In cells, closely spaced miRNA target sites within an mRNA can act cooperatively, leading to more repression of the target mRNA than expected by independent action at each site. Using purified miRNA–AGO2 complexes, synthetic target RNAs, and a purified domain of TNRC6B (GW182 in flies) that is able to simultaneously bind multiple AGO proteins, we examined both the occupancies and binding affinities of miRNA–AGO2 complexes and target RNAs with either one site or two cooperatively spaced sites. On their own, miRNA–AGO2 complexes displayed little if any cooperative binding to dual sites. In contrast, in the presence of the AGO-binding region of TNRC6B, we observed strong cooperative binding to dual sites, with almost no singly bound target RNAs and substantially increased binding affinities and Hill coefficients. Competitive slicing experiments indicated that association rates between miRNA–AGO2 complexes and targets were not affected, which implied that the improved affinities were due to reduced dissociation. Thus, the multivalent binding of TNRC6 enables cooperative binding of miRNA–AGO complexes to target RNAs, thereby explaining the basis of cooperative action.

Introduction

MicroRNAs (miRNAs) are ~22-nt RNAs that associate with an Argonaute (AGO) protein

to form a complex that directs the posttranscriptional down-regulation of mRNAs (Bartel,

2009). Within this complex, the miRNA pairs to a site within an mRNA, typically within

its 3′ untranslated region (UTR), thereby specifying the mRNA to be repressed,

whereas AGO interacts with TNRC6, a scaffold protein that recruits the PAN2/PAN3

and the CCR4/NOT deadenylation complexes to the targeted mRNA.

The consequence of the ensuing deadenylation can differ, depending on the regulatory

regime operating in the cells (Subtelny et al., 2014). In early embryos, where mRNAs

with shorter tails are stable but translated less efficiently, translational repression is

observed. In either later embryos or postembryonic cells, where mRNAs with shorter

tails are decapped more rapidly but translated no less efficiently, mRNA destabilization

is observed. Some translational repression, attributable to the action of DDX6 and 4E-T,

which can be recruited by the CCR4/NOT complex (Jonas and Izaurralde, 2015), is

sometimes also observed in postembryonic cells, but mRNA destabilization explains

most of the repression observed for endogenous mRNAs of postembryonic cells

(Eichhorn et al., 2014).

Key to the interaction between AGO and TNRC6 are three tryptophan-binding pockets

on the surface of AGO (Sheu-Gruttadauria and MacRae, 2018). Indeed, the TNRC6

homolog of flies is named GW182 because of its abundant glycine (G) and tryptophan

(W) residues. The G and W residues fall primarily in a large, apparently unstructured N-terminal domain of TNRC6, which has three AGO-binding "hotspots" (Jonas and Izaurralde, 2015; Pfaff et al., 2013). Each of these hotspots has multiple W residues that are flanked by amino acids with small or flexible side chains, which help explain the affinity to AGO (Elkayam et al., 2017; Pfaff et al., 2013).

More than 60% of human mRNAs are conserved targets of miRNAs, and on average, each conserved target has 4–5 preferentially conserved miRNA sites (Friedman et al., 2009). Each of these sites typically has perfect pairing to the miRNA seed (miRNA positions 2–7), often supplemented by an additional pair to miRNA position 8 or an A across from miRNA position 1, or both (Bartel, 2009).

Analyses of the global effects of miRNAs on mRNA levels indicate that if an mRNA has multiple sites to the same miRNA, the observed repression ordinarily matches that expected if each site acted independently (Grimson et al., 2007). For example, if one site one its own reduces an mRNA level by 30% and the second site reduces it by 20%, the effect of both of them together would be expected to be 44% (1 − (0.7 X 0.8)). However, when two miRNA sites are close to each other, the observed repression typically exceeds that expected from the independent action of the two sites (Grimson et al., 2007; Saetrom et al., 2007). One study reports that the strongest cooperative action is observed when sites are < 40 nt apart (counting the number of nucleotides between the 3′ end of the upstream site and the 5′ end of the downstream

site) but > 7 nt apart, presumably because at very close distances binding of one complex occludes binding of the second (Grimson et al., 2007). Another study reports that the strongest cooperative action is observed when sites are between 13–35 nt apart (Saetrom et al., 2007).

The human transcriptome of 19,473 3′ UTRs has 18,156 instances of transcripts with sites to any of the broadly conserved miRNA families within the cooperative distance of 8–39 nt. 1,258,129 pairs of sites exist within this cooperative distance, of which, 21,375 were examples where both sites are to the same miRNA family. Here, we set out to explain the molecular basis of this cooperative action.

Results and Discussion

Synergistic action of closely spaced miRNA sites

Transfecting miRNAs into human cell culture results in repression of target mRNAs containing sites to the miRNAs. When a target has multiple sites closely spaced (within 100 nt as measured from the 3′ end of the first site to the 5′ end of the second site), that target exhibits greater repression than would be expected if the two miRNA sites acted independently (Fig. 1A).

In vitro analysis of miRNA site occupancy

Recent experiments have shown that repression efficacy correlates strongly with the binding affinity between the miRNA–AGO complex and its target sites (McGeary et al., 2018). With this observation in mind, we reasoned that the cooperative action of closely

spaced sites might be due to cooperative binding of miRNA–AGO complexes to two closely spaced sites. To test this idea, we set out to examine whether the miRNA–AGO complex binds cooperatively to an RNA target with two closely spaced sites.

Bulk binding affinities between miRNA–AGO complexes and their targets are typically measured using filter binding, in which a nitrocellulose membrane retains AGO and any associated RNA, thereby separating bound from unbound target RNA (Wee et al., 2012). However, because this method cannot distinguish target RNA bound by one complex from that bound by two, it cannot provide the occupancy information needed to measure binding cooperativity. Reasoning that a native electrophoretic mobility-shift assay (EMSA) would be able to provide the desired occupancy information, we explored the utility of this assay for examining binding affinity between the miR-1–AGO2 complex and its targets.
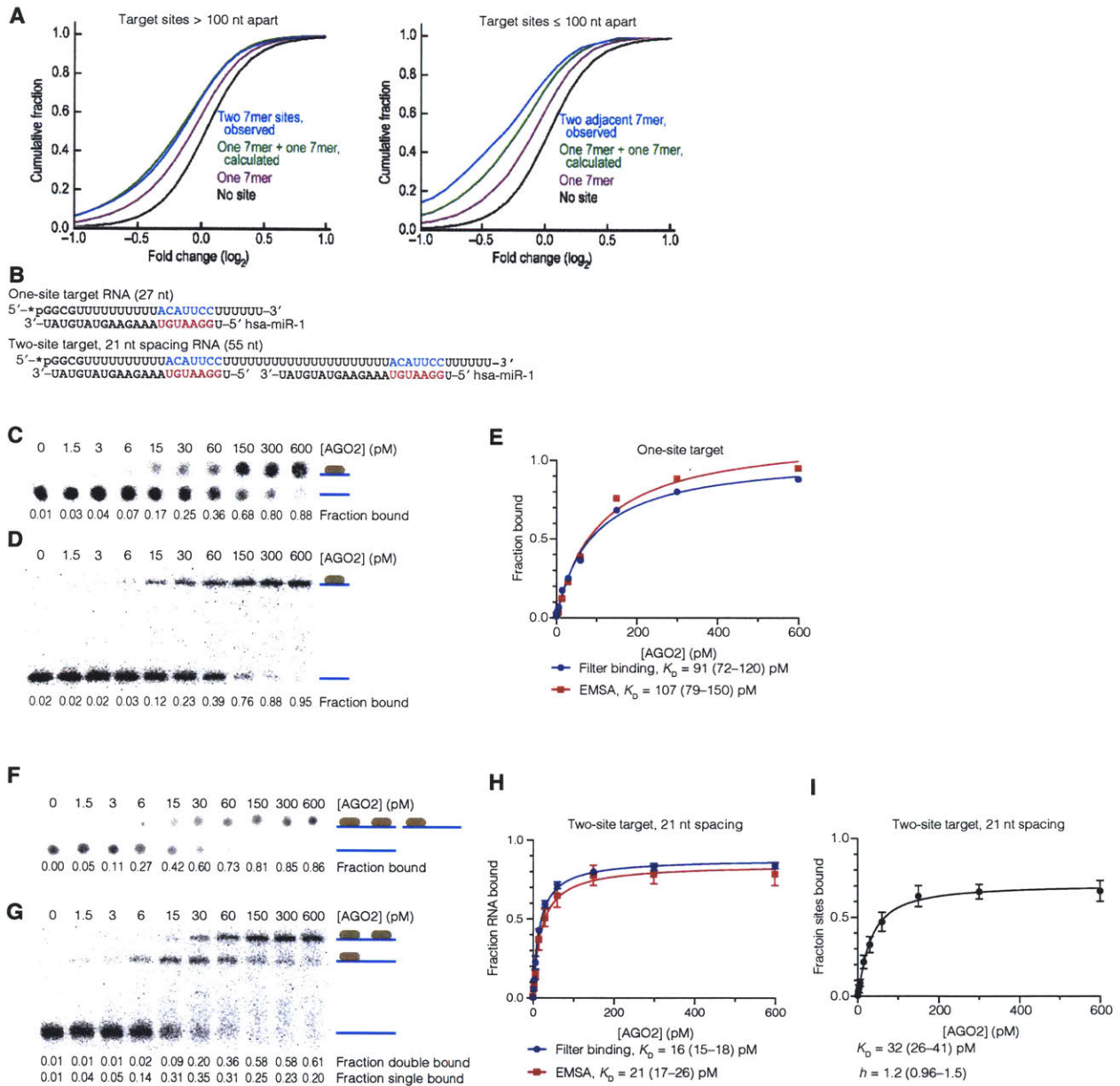
A

Target sites > 100 nt apart

Cumulative fraction vs Fold change (log₂)
- Two 7mer sites, observed
- One 7mer + one 7mer, calculated
- One 7mer
- No site

Target sites ≤ 100 nt apart

Cumulative fraction vs Fold change (log₂)
- Two adjacent 7mer, observed
- One 7mer + one 7mer, calculated
- One 7mer
- No site

B

One-site target RNA (27 nt)
5′-*pGGCGUUUUUUUUUUACAUUCCUUUUUU-3′
3′-UAUGUAUGAAGAAAUGUAAGGU-5′ hsa-miR-1

Two-site target, 21 nt spacing RNA (55 nt)
5′-*pGGCGUUUUUUUUUUACAUUCCUUUUUUUUUUUUUUUUUUUUUUACAUUCCUUUUUU-3′
3′-UAUGUAUGAAGAAAUGUAAGGU-5′ 3′-UAUGUAUGAAGAAAUGUAAGGU-5′ hsa-miR-1

C

0 1.5 3 6 15 30 60 150 300 600 [AGO2] (pM)

0.01 0.03 0.04 0.07 0.17 0.25 0.36 0.68 0.80 0.88 Fraction bound

D

0 1.5 3 6 15 30 60 150 300 600 [AGO2] (pM)

0.02 0.02 0.02 0.03 0.12 0.23 0.39 0.76 0.88 0.95 Fraction bound

E

One-site target

Fraction bound vs [AGO2] (pM)
- Filter binding, K_D = 91 (72–120) pM
- EMSA, K_D = 107 (79–150) pM

F

0 1.5 3 6 15 30 60 150 300 600 [AGO2] (pM)

0.00 0.05 0.11 0.27 0.42 0.60 0.73 0.81 0.85 0.86 Fraction bound

G

0 1.5 3 6 15 30 60 150 300 600 [AGO2] (pM)

0.01 0.01 0.01 0.02 0.09 0.20 0.36 0.58 0.58 0.61 Fraction double bound
0.01 0.04 0.05 0.14 0.31 0.35 0.31 0.25 0.23 0.20 Fraction single bound

H

Two-site target, 21 nt spacing

Fraction RNA bound vs [AGO2] (pM)
- Filter binding, K_D = 16 (15–18) pM
- EMSA, K_D = 21 (17–26) pM

I

Two-site target, 21 nt spacing

Fraction sites bound vs [AGO2] (pM)
K_D = 32 (26–41) pM
h = 1.2 (0.96–1.5)

Figure 1. Measuring affinity between miRNA–AGO2 and target RNA

(A) Cooperative action of closely spaced miRNA target sites. Changes in mRNA levels after miRNA transfection for messages containing the indicated combinations of miRNA binding sites. Panel from Fig. 1D and E from (Grimson et al., 2007). (B) Diagram of synthetic miR-1 targets with either one site or two sites. The 7-nt sites (blue) pair to miRNA positions 2–8 (red). (C) Binding of miR-1–AGO2 to its one-site target, as detected by filter binding. The top row shows the amount of labeled target retained with miR-1–AGO2 on the nitrocellulose filter, with the cartoon on right depicting the miRNA–AGO–target ternary complex (brown AGO2 bound to blue target). The bottom row shows the amount of labeled target that passed through the nitrocellulose filter and bound to the nylon filter, with the cartoon depicting free target (blue line). Shown are phosphorimager scans of the filters, which were used to calculate, for each

concentration of miR-1–AGO2, the fraction of target bound (indicated below the scans). (*D*) Binding of miR-1–AGO2 to its one-site target, as detected by EMSA. Otherwise, this panel is as in *C*. (*E*) Binding curves fit to the results of *C* and *D* (blue and red, respectively). Shown for each method are inferred K_D values with 95% confidence intervals in parentheses. (*F*) Binding of miR-1–AGO2 to its two-site target, as detected by filter binding. The cartoons on the right depict two AGO2 complexes bound to target (top left), one AGO2 complex bound to target (top right, shown bound to one site but also could be bound to the other site), and free target (bottom). Otherwise, this panel is as in *C*. (*G*) Binding of miR-1–AGO2 to its two-site target, as detected by EMSA. Otherwise, this panel is as in *F*. (*H*) Binding curves fit to three replicates of both *F* and *G* (blue and red, respectively). Otherwise, this panel is as in *E*. (*I*) The Hill curve fit to three replicates of *G*, showing the K_D and *h* values, with 95% confidence intervals in parenthesis.

We first measured the binding affinity between the complex and an RNA with a single

site. Human AGO2 loaded with human miR-1 was purified (Flores-Jasso et al., 2013;

McGeary et al., 2018) and its binding to a 27-nt RNA that had a site matching miR-1

nucleotides 2–8 (Fig. 1*B*) was examined. A range of miR-1–AGO2 concentrations were

incubated with trace target RNA, which was 5′-radiolabeled, and after reaching binding

equilibrium, the fraction of target bound was measured by both a filter-binding assay

and a native EMSA. The filter-binding assay was performed with stacked nitrocellulose

and nylon membranes, in which nitrocellulose membrane captured AGO and any

associated RNA, whereas the nylon captured unbound RNA (Fig. 1*C*). At each AGO2

concentration, the fraction of bound target observed by mobility shift resembled that

observed by filter binding (Fig. 1*C* and *D*). For both assays, simple binding curves fit

well to the results, and the K_D values inferred from these curves (91 and 110 pM,

respectively) were similar to each other (Fig. 1*E*) and fell within the range of values

determined for complexes involving other mammalian miRNAs and measured using

either filter-binding or single-molecule methods (Salomon et al., 2015; Wee et al., 2012).

Having established an EMSA for miR-1–AGO2 binding to target RNA, we used this assay to examine binding to a target that had two 7-nt sites separated by 21 nt, choosing an oligo(U) spacer to avoid secondary structure within the target RNA (Fig. 1*B*). As anticipated, the EMSA distinguished between free RNA, RNA bound by one miR-1–AGO2 complex, and RNA bound by two miR-1–AGO2 complexes (Fig. 1*F*). Moreover, when considering the fraction of target bound to at least one complex, results of the EMSA agreed well with those of the filter-binding assay (Fig. 1 *F–H*).

The distinctly identifiable binding states observed with the EMSA allowed fitting of the Hill equation, producing a Hill coefficient, *h*, used to describe the cooperativity of binding in systems with multiple simultaneous binding events. An *h* of 1.0 indicates no cooperativity, whereas, an *h* less than or greater than 1.0 indicates negative or positive cooperativity, respectively. Because the target had two miRNA target sites, an *h* of 2 would indicate maximal positive cooperativity. Fitting the Hill equation to the EMSA results for a 2-site target yielded an *h* of 1.2, with a 95% confidence interval (CI) of 0.96–1.5 (Fig. 1*I*). Thus, although the possibility of some cooperative binding cannot be excluded, these results did not provide compelling evidence for the cooperative binding of miR-1–AGO2 to a 2-site target in the absence of additional factors.

Enhanced cooperativity of AGO2 binding in the presence of TNRC6

TNRC6 has an extended AGO-binding domain with potential to bind more than one AGO (Takimoto et al., 2009). Indeed, within the AGO-binding domain of TNRC6B, one of the three TNRC6 paralogues in humans, three non-overlapping AGO-binding hotspots have been mapped (Pfaff et al., 2013), and one molecule of TNRC6A can simultaneously bind three AGO proteins (Elkayam et al., 2017). This ability to bind more than one AGO protein has led to speculation that TNRC6 might link multiple miRNA–AGO complexes simultaneously bound to different sites of a target, thereby imparting cooperative binding to such targets with multiple suitably spaced sites (Elkayam et al., 2017; Hauptmann et al., 2015; Pfaff et al., 2013; Takimoto et al., 2009).

With an assay for examining the cooperativity of miRNA–AGO-binding to targets, we were positioned to test the idea that the AGO-binding domain of TNRC6 might impart cooperative binding. For these studies, we overexpressed and purified the AGO-binding domain of TNRC6B. The recombinant construct, named 6B-ABD, included a region of TNRC6B containing residues 162–996, fused at its N terminus with maltose-binding protein (MBP) and at its C terminus with His$_6$, which were appended to enhance protein solubility and facilitate purification, respectively (Fig. 2A).

To examine how binding of 6B-ABD affected migration of miRNA–AGO2–target complexes, we designed a system that enabled control of the number of target sites bound to miRNA–AGO2. This system used a target with both a miR-1 site and a miR-

124 site (again separated by a 21-nt oligo(U) spacer), and to this 2-site target purified

miR-124–AGO2 or miR-1–AGO2 could be added to generate singly bound target, or

both miRNA–AGO2 complexes could be added to generate doubly bound target (Fig

2B). 6B-ABD was then added to these singly or doubly bound targets, and migration in

the EMSA was assessed (Fig. 2*B*). Adding 1 nM 6B-ABD to target bound by either miR-

1–AGO2 or miR-124–AGO2 only slightly reduced mobility of the target complex,

whereas adding 1 nM 6B-ABD to target bound by both miR-1–AGO2 and miR-124–

AGO2 substantially reduced mobility of the target complex, a small portion of which

failed to migrate into the gel. These results demonstrated the ability to detect

association of 6B-ABD to target bound by two miRNA–AGO2 complexes.
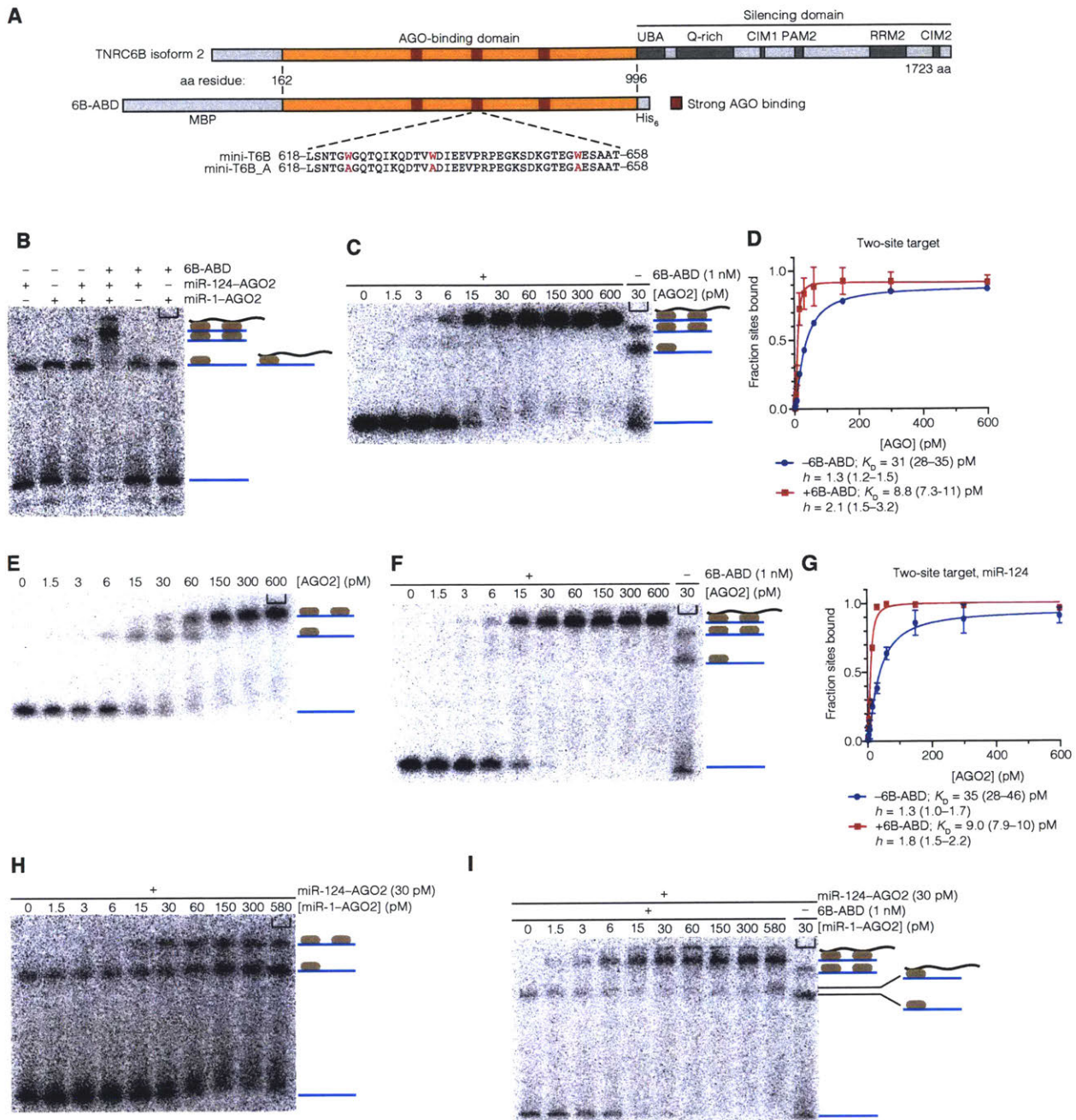
Figure 2. The effects of 6B-ABD on miRNA–AGO2 binding to two-site targets

(*A*) Domain structure of TNRC6B and its derivatives. At the top is TNRC6B isoform 2, with its AGO-binding domain colored orange and the mapped high-affinity binding regions colored red. Below TNRC6B is 6B-ABD, which contained the TNRC6B AGO-binding domain flanked by the maltose-binding domain (MBP) and a His$_6$ tag. Below 6B-ABD are the mini-T6B and mini-T6B_A synthetic peptides. (*B*) Assessment of target migration in the EMSA following combinatorial addition of miRNA–AGO and 6B-ABD. On the right, cartoons depict (top to bottom): target (blue) bound by two miRNA–AGO2

56

complexes (brown) that are bound by 6B-ABD (black), target bound by two miRNA–AGO2 complexes, target bound by one miRNA–AGO2 complex (either miR-1–AGO2 or miR-124–AGO2 but only one of the two possibilities shown for simplicity), and target bound by one miRNA–AGO2 complex that is bound by 6B-ABD (which essentially co-migrates with target bound by one miRNA–AGO2 complex that is not bound by 6B-ABD), and free target. The three-sided box in upper right corner of the gel shows the location of well. (C) The effect of 6B-ABD on the binding of miR-1–AGO2 to its two-site target. 1 nM 6B-ABD was included in each binding reaction, except the one run on the far-right lane. Cartoons on the right are as in B. Otherwise, this panel is as in Fig. 1G. (D) The effect of 6B-ABD on the binding of miR-1–AGO2 to its two-site target, as evaluated by the Hill equation. The Hill equation is fit to two replicates of C (red) and to EMSA results for the analogous binding reactions performed in the absence of 6B-ABD (blue). K_D and h values are indicated for each fit, with 95% confidence intervals in parenthesis. (E) Binding of miR-124–AGO2 to its two-site target. Otherwise, this panel is as in Fig. 1G. (F) The effect of 6B-ABD on the binding of miR-124–AGO2 to its two-site target. Otherwise, this panel was as in C. (G) Hill equation fit to two replicates of E and F (blue and red, respectively). Otherwise, this panel is as in D. (H) Binding of miR-1–AGO2 and miR-124–AGO2 to a target with one site to each miRNA. miR-1–AGO2 was titrated into reactions that contained 30 pM miR-124–AGO2. Otherwise, this panel is as in E. (I) The effect of 6B-ABD on the binding of miR-1–AGO2 and miR-124–AGO2 to a target with one site to each miRNA. miR-1–AGO2 was titrated into reactions that contained 30 pM miR-124–AGO2. Otherwise, this panel is as in C.

Having established how adding 6B-ABD influences migration of different miRNA–AGO2–target complexes, we investigated how 6B-ABD influences the binding of miR-1–AGO2 to its 2-site target RNA. Compared to binding reactions without 6B-ABD (Fig. 1B), adding 1 nM 6B-ABD nearly eliminated the singly bound species (Fig. 2C), with the doubly bound target dominating over the singly bound target at much lower miR-1–AGO2 concentrations (as low as 6 pM compared to > 60 pM). This altered behavior observed upon adding the TNRC6B AGO-binding domain was precisely that expected when shifting from noncooperative to highly cooperative binding. Indeed, when fitting the Hill equation, the occupancy observed upon adding 6B-ABD yielded an h of 2.1

(95% CI, 1.5– 3.2) (Fig. 2D). We conclude that TNRC6 substantially increases the cooperativity of miR-1–AGO2 binding to a 2-site target RNA.

To examine if the observed cooperativity depended on the identity of the miRNA, we repeated the experiments with miR-124–AGO2 and a cognate target with two sites to miR-124 separated by a 21-nt oligo(U) spacer. The results resembled those observed for miR-1; the singly bound species observed without 6B-ABD was nearly undetectable in the presence of 6B-ABD, and the doubly bound target dominated over the singly bound target at much lower miR-124–AGO2 concentrations (Fig. 2 E and F). In the absence of 6B-ABD the Hill coefficient was 1.3 (95% CI, 1.0–1.7), which increased to 1.8 (95% CI, 1.5–2.2) with the addition of 6B-ABD (Fig. 2G).

Because most cooperatively spaced sites in endogenous 3' UTRs correspond to different miRNAs, we also tested whether the TNRC6B AGO-binding domain could enhance cooperative binding to a target with sites to two different miRNAs, specifically, a miR-1 site 21 nt from a miR-124 site. miR-124–AGO2 was set at 30 pM, a concentration that led to partial occupancy of the miR-124 site, and miR-1–AGO2 was titrated in, either in the absence or in the presence of 6B-ABD (Fig. 2 H and I). Clear hallmarks of increased cooperativity were observed in the presence of 6B-ABD. For example, at 30 pM miR-124–AGO2, 15 pM miR-1–AGO2 and in the absence of 6B-ABD, 68% of target RNA was free, 19% was bound by one miRNA–AGO2 complex, and 13% was bound by two complexes, whereas in the presence of 6B-ABD, free target

decreased to 18%, singly bound target decreased to 17%, and doubly bound target increased to 65% (Fig. 2 *H* and *I*). Thus, TNRC6 can mediate cooperative binding involving two AGO proteins, each loaded with a unique miRNA.

Site spacing

Previous studies examining the efficacy of repression in the cell indicate that either 8–39 or 13–35 nt between the 3' end of the first site and the 5' end of the second site provide optimal spacing for miRNA cooperative action, raising the question of whether such a range also applies to binding cooperativity in vitro (Grimson et al., 2007; Saetrom et al., 2007). To test intersite spacing above the previously defined boundaries, we created a target with a 60-nt oligo(U) spacer. Using this target in the absence of 6B-ABD, three binding states were observed: free target, target bound by a single miR-1–AGO2, and target bound by two miR-1–AGO2 complexes (Fig. 3*A*), whereas in the presence of 6B-ABD, target bound by a single miR-1–AGO2 was difficult to detect at any point in the concentration course—a hallmark of cooperative binding (Fig. 3*B*). Fitting the binding curves indicated that in the absence of 6B-ABD, miR-1–AGO2 bound target RNA with K_D = 24 pM and h = 1.4 (95% CI, 0.94–2.0), whereas in the presence of 6B-ABD, miR-1–AGO bound target with K_D = 9.1 pM with h = 1.8 (95% CI, 1.3–2.6) (Fig. 3*C*), also supporting the conclusion that 6B-ABD increased the affinity and cooperativity of binding.

These results showed that cooperative binding can be achieved at a linker length of 60 nt, which exceeded the 56-nt linker length for which cooperativity is not observed

in cells using a reporter assay (Grimson et al., 2007). Factors that might explain this difference include the different linker and flanking sequences and the milieu of RNA-binding proteins present in cells but absent in our purified system, which might effectively iron out the target mRNA and increase the three-dimensional distance between sites.

To test an intersite spacing below the previously defined boundaries, we generated a 2-site target with a miR-1 site placed 4 nt from a miR-124 site. In the absence of 6B-ABD, binding of only one miRNA–AGO2 complex to the target was detected, with a K_D of 88 pM, whereas in the presence of 6B-ABD, the same was observed, with a similar K_D of 140 pM (Fig. 3*D–F*). The binding of only one miRNA–AGO2 complex to this target with closely spaced sites was presumably due to a steric clash that precluded binding of a second complex. This apparent inability of two AGO proteins to simultaneously associate with the target explained the lack of cooperative binding. This mechanism for preventing cooperativity would presumably be difficult to attenuate with altered sequences or RNA-binding proteins, which explains why our result in vitro matched that observed for closely spaced sites when using reporter assays in cells (Grimson et al., 2007; Saetrom et al., 2007).
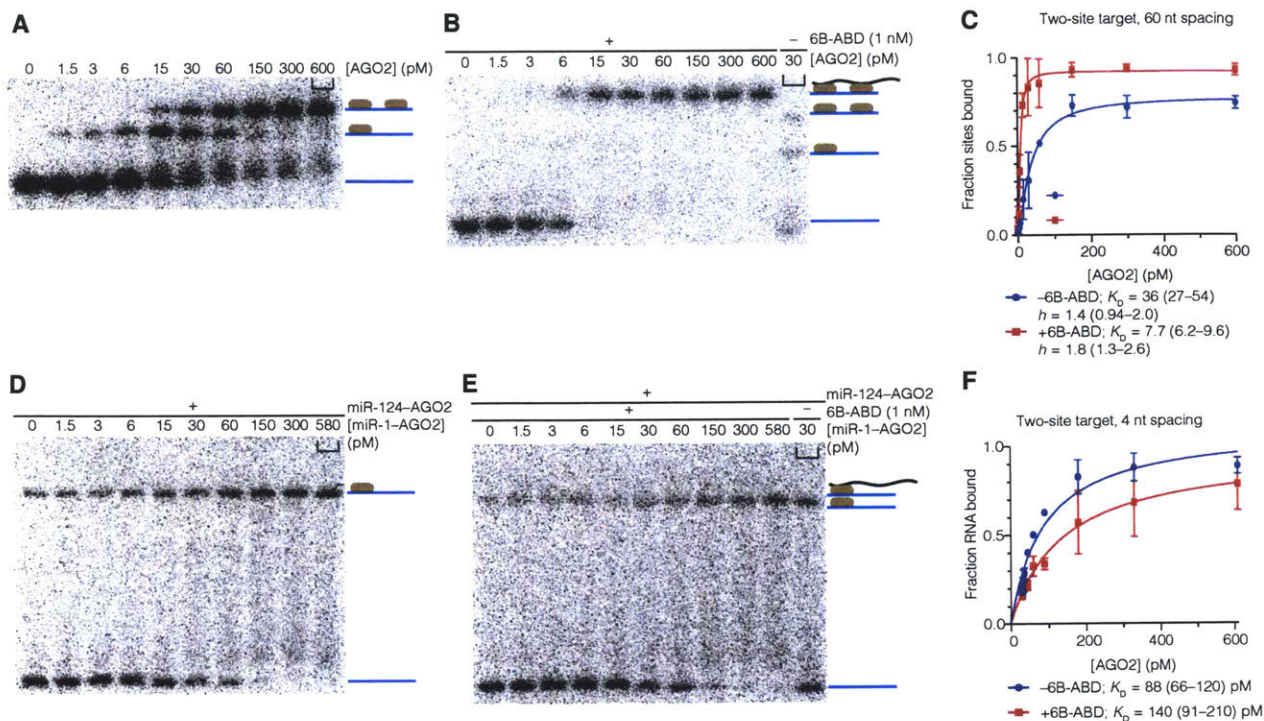
Figure 3. Assessing cooperative binding at different site-spacing distances
(*A*) Binding of miR-1–AGO2 to a target with two sites spaced 60 nt apart, as detected by EMSA. Otherwise, this panel is as in Fig. 1*F*. (*B*) The effect of 6B-ABD on the binding of miR-1–AGO2 to a target with two sites spaced 60 nt apart. Otherwise, this panel was as in Fig. 2*C*. (*C*) The effect of 6B-ABD on the binding of miR-1–AGO2 to a target with two sites spaced 60 nt apart, as evaluated by the Hill equation. The Hill equation was fit to two replicates of *A* and *B* (blue and red, respectively). Otherwise, this panel is as in Fig. 2*D*. (*D*) Binding of miR-1–AGO2 and miR-124–AGO2 to a target with closely spaced sites to each miRNA. miR-1–AGO2 was titrated into reactions that contained 30 pM miR-124–AGO2. Otherwise, this panel is as in Fig. 2*H*. (*E*) The effect of 6B-ABD on the binding of miR-1–AGO2 and miR-124–AGO2 to a target with closely spaced sites to each miRNA. Target bound by one miRNA–AGO2 complex (either miR-1–AGO2 or miR-124–AGO2 but only one of the two possibilities shown for simplicity) migrates slightly faster than target bound by one miRNA–AGO2–6B-ABD complex. Otherwise, this panel is as in Fig. 2*I*. (*F*) Binding curves fit to two replicates of *D* and *E* (blue and red, respectively). Shown for each curve are inferred K_D values with 95% confidence intervals in parentheses.

Disrupting cooperative binding

6B-ABD had the three known AGO-binding hotspots of TNRC6B, consistent with the hypothesis that the ability of 6B-ABD to bind multiple AGO proteins simultaneously provided the basis for cooperative binding of AGO to target RNA. To evaluate this hypothesis that cooperativity depended on multiple and specific AGO–TNRC6 interactions, we generated a synthetic peptide designed to bind only one AGO protein and examined whether this peptide could disrupt cooperative binding. Our peptide was a smaller version of the T6B peptide, an 85-aa peptide that corresponds to residues 599–683 of TNRC6B and is known to bind strongly to AGO (Hauptmann et al., 2015; Pfaff et al., 2013) (Fig. 2A). Our peptide, called "mini-T6B," included a 41-aa fragment of T6B that corresponded to residues 618–658 of TNRC6B. Mini-T6B was designed to included only three tryptophan residues, reasoning that such a peptide could interact with each of the tryptophan-binding pockets on one AGO molecule but would lack additional tryptophan residues that might interact with another AGO. As a control, a second peptide, called "mini-T6B_A" was designed in which the three tryptophan residues of mini-T6B were changed to alanine (Fig. 2A).

The effect of mini-T6B was tested on miR-1–AGO2 binding to a target with two miR-1 sites spaced 21 nt apart (Fig. 1B), setting the concentration of miR-1–AGO2 to 30 pM, at which free target RNA, target RNA bound by one miR-1–AGO2, and target RNA bound by two miR-1–AGO2 complexes were clearly observed. When adding a high concentration of mini-T6B or mini-T6B–A to the reaction, neither peptide affected the mobility of the complexes (Fig. 4B). However, when repeating the experiment in the

presence of 1 nM 6B-ABD, which normally imparts cooperative binding of miR-1–AGO2 under these conditions, mini-T6B disrupted the cooperative behavior, as indicated by the reappearance of singly bound target (Fig. 4 C and D). EMSA lane 1 shows EMSA of miR-1–AGO2 binding to 2-site target, 21 nt apart, in the absence of 6B-ABD. Lane 2 is the same as lane 1, but with the addition of 6B-ABD. Target has super-shifted and singly bound target species is depleted. Lane 3 shows the addition of mini-T6B to the conditions in lane 2. Note the reappearance of singly bound target, a greater amount of free target, and a decrease in doubly bound target. Lane 4 shows the addition of mini-T6B_A to the same conditions as lane 2. Note the similarity between lanes 2 and 4; a similar amount of mini-T6B_A used in lane 4, as compared to mini-T6B in lane 3, did not disrupt the cooperative behavior, as expected if the behavior was mediated specifically through tryptophan residues binding to AGO2. These results supported the conclusion that simultaneous binding of TNRC6 to multiple miRNA–AGO2 complexes enables cooperative binding to targets that have suitably spaced miRNA sites. The high concentration of mini-T6B required to displace 6B-ABD from the two-site target bound by two miRNA–AGO complexes indicates that the truncated peptide does not perfectly recapitulate the interactions of the entire ABD.
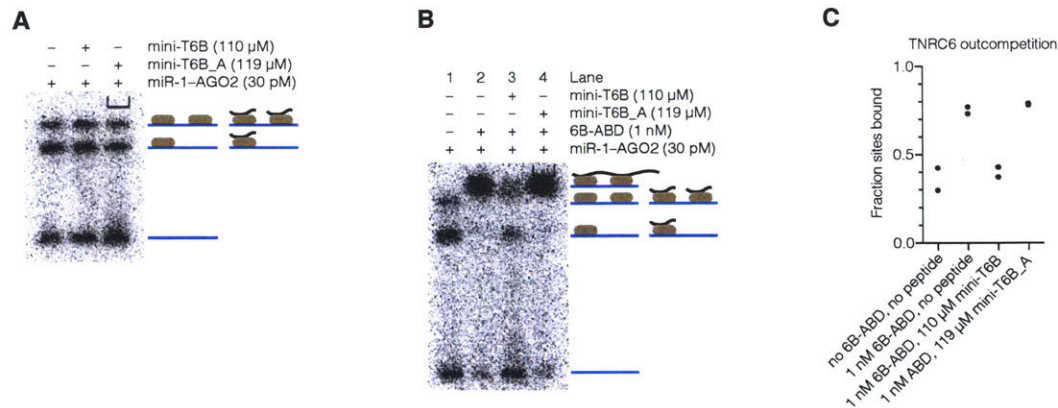
Figure 4. Disrupting cooperative binding
(*A*) The effect of mini-T6B or mini-T6B_A on the binding of miR-1–AGO2 to its two-site target with 21 nt between sites. In cartoons, the short black line represents mini-T6B1 or mini-T6B_A. Otherwise this panel in as in Fig. 1*G*. (*B*) The effect of mini-T6B or mini-T6B_A on the binding of miR-1–AGO2 to its two-site target in the presence of 1 nM 6B-ABD. In cartoons, short black line represents mini-T6B1 or mini-T6B_A. Otherwise as in Fig. 2*C*. (*C*) Quantification of two replicates of *B*.

TNRC6 slows the dissociation rate of cooperatively bound miRNA–AGO2 complex

TNRC6 might impart cooperative binding by either increasing the association rate constant (k_{on}) between miRNA–AGO and target, slowing the dissociation rate constant, (k_{off}) or both. To distinguish between these possibilities, we designed and implemented a competitive slicing assay that was sensitive to differences in k_{on} but not k_{off}. One of the two slicing substrates was a 22-nt RNA that was perfectly complementary to miR-1; it was a substrate for AGO2-catalzyed slicing but could not benefit from cooperative binding because it had only one site to the miRNA (Fig. 5*A*). The other slicing substrate was a 55-nt RNA that had two miR-1 sites separated by a 20-nt oligo(U) linker, one of which was a slicing-competent 22-nt site perfectly complementary to miR-1 and the other of which matched miR-1 nucleotides 2–8 (Fig. 5*A*).

64

These substrates were combined and added, each target in 10-fold excess over miR-1–AGO2, in either the presence or absence of 6B-ABD, and the generation of slicing products was measured. In this regime, the two substrates were competing for binding to limiting miR-1–AGO2, and because slicing of the perfectly complementary site is much more rapid than dissociation of miR-1–AGO2 from this perfectly complementary site (Chen et al., 2017; Wee et al., 2012), the binding competition was based primarily on relative association rates. Thus, if 6B-ABD acts to increase k_{on} of miR-1–AGO2 to the 2-site target, then the presence of 6B-ABD would be expected to enhance binding to, and slicing of, the 2-site target as compared to the 1-site target (Fig. 5*B*). If, however, 6B-ABD does not act to increase k_{on} of miR-1–AGO2 to the 2-site target, then the presence of 6B-ABD would not be expected to influence the slicing of the 2-site target as compared to the 1-site target.

We observed that 6B-ABD did not preferentially enhance slicing of the 2-site target but rather slightly decreased slicing of both targets. (Fig. 5 *C* and *D*). With this undetectable influence on k_{on}, we conclude that slowed k_{off} between miRNA–AGO and its suitably spaced sites must be the primary cause of the cooperative binding observed in the presence of 6B-ABD. Thus, TNRC6 helps maintain the binding of two miRNA–AGO complexes to a two-site target once they are already associated but does little to help recruit the second miRNA–AGO to the second site of a target. The notion that multivalent binding of TNRC6 to miRNA–AGO is consequential primarily only after the miRNA–AGO complexes have already associated with target would be even more relevant in the cell, where the high diversity of miRNAs would lower the probability that

the second miRNA–AGO complex that might interact with TNRC6 prior to interacting

with target would also happen to match the second target site.

A

55 nt RNA target, 45 nt slicing product
5′–*pUUUUUUACAUUCCUUUUUUUUUUUUUUUUUUUAUACAUACUUCUUUACAUUCCA–3′
3′–UAUGUAUGAAGAAAUGUAAGGU–5′   3′–UAUGUAUGAAGAAAUGUAAGGU–5′ hsa-miR-1

22 nt RNA target, 12 nt slicing product
5′–*pAUACAUACUUCUUUACAUUCCA–3′
3′–UAUGUAUGAAGAAAUGUAAGGU–5′ hsa-miR-1

B

In the presence of 6B-ABD, increased k_{on} to two-site target over one-site target

$k_{on, two-site}$

$k_{on, one-site}$

slicing

In the absence of 6B-ABD, equal k_{on} of one- and two-site targets

$k_{on, two-site}$

$k_{on, one-site}$

slicing

Legend

miR-1–AGO2 | Two-site target (55 nt) | One-site target (22 nt) | 6B-ABD | Slicing product of one-site target (45 nt) | Slicing product of two-site target (12 nt) | Slicing product of one- or two-site target (12 nt, not visible on gel)

C

D

Competitive cleavage assay

- 55 nt –6B-ABD   slope = 0.010
- 55 nt +6B-ABD   slope = 0.0097
- 22 nt –6B-ABD   slope = 0.0078
- 22 nt +6B-ABD   slope = 0.0069

E

Figure 5. TNRC6 slows the dissociation rate of cooperatively bound miRNA–AGO2 complex

(*A*) Diagram of slicing targets. The two-site slicing target has two miR-1 sites spaced 20 nt apart. The 5′ site is only competent for binding, whereas the 3′ site competent for binding and slicing. Slicing of this target generates a 45-nt 5′ product (purple) and a 10-nt 3′ product (blue). The one-site slicing target has one miR-1 site, which is competent for slicing. Slicing generates a 12-nt 5′ product (purple) and 10-nt 3′ product. (*B*) Schematic of a competitive slicing experiment designed to detect an influence of 6B-ABD on the association of miRNA–AGO2 and target. Limiting miRNA–AGO is incubated with excess one-site and two-site targets. In the presence of excess 6B-ABD (top), miRNA–AGO2 preferentially associates with two-site target. Once associated with target, slicing occurs much more rapidly than dissociation, and to the extent that 6B-ABD enhances the association rate constant (k_{on}), this slicing generates more 45-nt product than 12-nt product. (For simplicity, miRNA–AGO2 and 6B-ABD are not depicted with the cleaved target and remaining target on the right.) In the absence of 6B-ABD (bottom), miR-1–AGO2 associates with one- and two-site targets equally, and thus slicing generates similar amounts of 45-nt and 12-nt products. (*C*) Results for the competitive slicing experiment diagramed in *B*. 5 pM miR-1–AGO2 was incubated with 50 pM 5′-radiolabeled one-site target and 50 pM 5′-radiolabeled two-site target. At the times indicated, the reaction was stopped, and targets and products were resolved on a denaturing gel. Shown is a phosphorimager scan of the gel. Left lane, decade RNA ladder. Cartoons of labeled RNA species to the right of gel are as in *B*. (*D*) Quantification of the results of the competitive slicing experiment, indicating that 6B-ABD does not detectably increase the k_{on} for the two-site target. Lines show the linear fit (with slope indicated) to the results in *C*, with an additional replicate of early time points. (*E*) Model for cooperative binding of both a two-site target (vertical axis) and TNRC6 (horizontal axis). Two AGO proteins (brown) loaded with miRNAs (red) associate with target mRNA (blue) that has cooperatively spaced target sites. TNRC6 (black) associates with both AGO proteins via TNRC6 tryptophan residues (W).

Model for the cooperative binding and cooperative action of miRNAs

Our results point to a model in which TNRC6 confers cooperative binding of miRNA–AGO to appropriately spaced sites on target mRNAs (Fig. 5*E*). In this model, individual miRNA–AGO complexes first bind target RNA, typically without the help of TNRC6, and then TNRC6 associates with these target-bound miRNA–AGO proteins. Although TNRC6 does not change the microscopic dissociation rate of an individual miRNA–AGO bound to its site, TNRC6 does help to keep it tethered close to the target, such that if one of the two miRNA–AGO complexes dissociates from its site, then TNRC6 in

conjunction with the other miRNA–AGO keeps the dissociated miRNA–AGO in close proximity to the site and thereby at a high local concentration, facilitating re-binding (Fig. 5E, vertical axis). Likewise, the multivalent association of TNRC6 with the higher-order complex presumably helps prevent complete dissociation of TNRC6 (Fig. 5E, horizontal axis). Thus, the entire TNRC6–2x(miRNA–AGO) complex has a slower dissociation from target. With this slower dissociation, the repressive machinery associated with TNRC6 is tethered to the target mRNA for more time and thus has more time to deadenylate and translationally repress the target mRNA.

Although our experiments focused on targets bound to only one or two miRNA-AGO complexes, the ability of TNRC6 to simultaneously bind three complexes allows the model to be readily extended to targets with three sites (Elkayam et al., 2017). Moreover, increased phase separation observed upon adding AGO to a solution containing the TNRC6B AGO-binding domain suggests that AGO might have the ability to simultaneously interact with multiple TNRC6 molecules, albeit with presumably lower affinity to each molecule, which allows the model to extend to much higher-order complexes (Sheu-Gruttadauria and MacRae, 2018). Nonetheless, our results show that strong cooperative binding can be achieved without formation of higher-order assemblies.

Materials and Methods

miRNA duplexes

RNAs representing the guide and passenger strands of each miRNA duplex (Table S1) were chemically synthesized (IDT). Passenger strands were synthesized with a 5'-monophosphate, whereas guide strands were synthesized with a 5'-OH. Guide strands were 5'-monophosphorylated using T4 Polynucleotide Kinase (NEB, M0201S) and a small amount of ATP [γ-^{32}P] (PerkinElmer, NEG035C001MC). The reaction was desalted with a P-30 column (BioRad 7326251). Each RNA was then purified on a denaturing 15% acrylamide gel and resuspended in water. Two strands of a duplex were mixed with each other (870 pmol of each RNA) in annealing buffer (74 μl reaction with 30 mM Tris pH 7.5, 100 mM NaCl, and 1 mM EDTA) and heated to 90°C on a heat block, which was then allowed to cool to 35°C by sitting at room temperature for 90 min. NaCl was then added to a concentration of 0.39 M, and RNA was EtOH precipitated and resuspended in 10 μl annealing buffer. Duplex was then purified on a native 15% acrylamide gel that had been pre-run for 10 min. Purified duplex RNA was EtOH precipitated and resuspended in 10 μl annealing buffer.

miRNA–AGO2 preparation

Complexes of a specific miRNA–AGO2 were prepared as described, using an approach based on that of Flores-Jasso et al. (Flores-Jasso et al., 2013; McGeary et al., 2018). 3xFLAG–hAGO2 in a pcDNA3.3 construct was transfected into ~90% confluent HEK293T cells using Lipofectamine 2000, per manufacturer instructions. After two days of growth, S100 cytosolic extract was harvested as described (Wee et al., 2012), except

that cells were lysed in their hypotonic solution by being passed through a 23 Gauge

needle ~20 times. S100 extract was then brought to 13% glycerol (w/v) and snap frozen

in liquid nitrogen and stored in liquid nitrogen.

Gel-purified miRNA duplex was added to 1200 μl of S100 lysate to a final

concentration of 50 nM. After incubating at 25 °C for 2 h to allow cellular machinery to

load 3xFLAG–AGO2, the lysate was added to 200 μl of a slurry of magnetic beads

(Dynabeads MyOne Streptavidin C1, Invitrogen 65001) pre-bound to 500 pmol of a 3′

biotinylated capture oligo bearing an 8-nt site to the miRNA (Table S1), per

manufacturer protocol, except the washed oligo-bound beads were resuspended in

equilibration buffer (18 mM HEPES pH 7.4, 100 mM KAc, 3 mM MgAc, 0.01% IGEPAL

CA-630 (Sigma I8896), 0.2 mg/ml BSA (NEB B9000S), and 0.01 mg/ml yeast tRNA

(Life Technologies 15401-011)). After incubating at 22°C for 1 h with agitation, beads

were collected and washed five times in 400 μl equilibration buffer and five times in 200

μl high-salt equilibration buffer (18 mM HEPES pH 7.4, 2 M KAc, 3 mM MgAc, 0.01%

IGEPAL CA-630, 0.2 mg/ml BSA, and 0.01 mg/ml yeast tRNA). Captured miRNA–

AGO2 complex was eluted by resuspending the beads in 200 μl high-salt equilibration

buffer containing 10 μM competitor DNA oligo (Table S1), which was complementary to

the capture oligo. After incubating at 22°C for 2 h with agitation, the eluate was

collected, supplemented with 50 μl of glycerol buffer (18 mM HEPES pH 7.4, 100 mM

KAc, 1 mM MgAc, 0.01% IGEPAL CA-630, 0.2 mg/ml BSA, 0.01 mg/ml yeast tRNA, and

30% glycerol v/v), snap frozen in liquid nitrogen, and stored at −80°C.

Eluate was thawed and added to 20 μl of Anti-FLAG M2 magnetic beads (Sigma

M8823), which had been prepared by washing three times with equilibration buffer.

After incubation at 22°C for 2 h with agitation, beads were washed 3 times with 200 μl

equilibration buffer. Beads were then incubated in 60 μl equilibration buffer

supplemented with 146 μg/ml 3x FLAG peptide (Sigma F4799) at 22°C for 1 h with

agitation. The eluate was collected, supplemented with 0.4 μl 1 M DTT and 20.1 μl 80%

glycerol (v/v), snap frozen in liquid nitrogen, and stored at –80 °C.

Cloning of 6B-ABD

pFRT/TO/FLAG/HA-DEST TNRC6B was a gift from Thomas Tuschl (Addgene plasmid

#19884) (Landthaler et al., 2008). TNRC6B residues 162–996 were amplified and

appended to a His$_6$ tag using appropriate primers (Table S1) (Q5 High-Fidelity DNA

Polymerase, NEB E0555S) and then inserted into the pMAL-c5X vector (NEB N8108S)

using Gibson assembly per manufacturer instructions (NEB E5510S). Plasmids were

transformed into NEB 5-alpha Competent *E. coli* cells (NEB C2987I) and screened for

the correct insert by Sanger sequencing. Verified plasmid was transformed into

BL21DE3 *E. coli.* (Agilent 200131). The next day, a colony was picked and used to

generate a glycerol stock, which was stored at –80°C.

Expression and purification of 6B-ABD

A small scraping of glycerol stock was used to inoculate 5 ml LB, which was grown

under ampicillin selection at 37°C overnight on a shaker. This 5 ml culture was then

used to inoculate 4 x 500 ml cultures of LB, which were grown under ampicillin selection

at 37°C on a shaker to OD$_{600}$ of 0.6. Cultures were transferred to 20°C and induced with

IPTG (0.4 mM final concentration) and grown at 20°C on a shaker overnight (~16 h).

Cultures were combined into 2 x 1000 ml bottles and centrifuged at 4000g for 15 min at

4°C. Pellets were resuspended in 50 ml water, then centrifuged at 4000g for 5 min at

4°C. Pellets were resuspended in 47.5 ml lysis buffer (20 mM Tris pH 7.5, 150 mM

NaCl, 5% glycerol, 2 mM 2-mercaptoethanol, 0.1% IGEPAL CA-630, cOmplete EDTA-

free Protease Inhibitor Cocktail (1 tablet per 50 ml buffer) (Roche 11873580001), and

the suspension was sonicated six times (Branson Sonifier 250, 6 cycles of 50% output,

1 s on, 1 s off, 2 min) in a cold room on ice. Lysed samples were cleared by

centrifugation at 50000g for 30 min at 4 °C, and cleared lysate was added to Ni-NTA

agarose beads (Qiagen 30210), prepared by removing 500 μl of bead slurry, adding 2

ml lysis buffer, centrifuging at 2000g for 1 min, and removing supernatant. After gently

rocking in a cold room at 5.5°C for 105 min, samples were poured into a gravity-flow

poly-prep chromatography column, which was washed with 25 ml wash buffer (20 mM

Tris pH 7.5, 150 mM NaCl, 5% glycerol, 20 mM imidazole pH 7.5, 2 mM 2-

mercaptoethanol, 0.1% IGEPAL CA-630). Protein was was eluted with 5 ml elution

buffer (20 mM Tris pH 7.5, 150 mM NaCl, 5% glycerol, 200 mM imidazole pH 7.5, 2 mM

2-mercaptoethanol, 0.1% IGEPAL CA-630), and 4.7 ml of eluate was recovered and

concentrated in a 100 kDa centrifugal filter unit (Amicon UFC910024) to 340 μl by

centrifuging at 5000g for 21 min at 4°C. 160 μl gel-filtration buffer (18 mM HEPES pH

7.4, 100 mM KAc, 1 mM MgAc, 0.01% IGEPAL CA-630, 19.5% glycerol (v/v), 5 mM

DTT) was added to the concentrated sample for a final volume of 500 μl. The

concentrated sample was cleared by centrifugation at 21,130g for 5 min in a cold room

at 5.5°C and transferred to a new tube. The cleared sample was loaded onto a Superose 6 Increase 10/300 GL FPLC column (GE Life Sciences 29091596) pre-equilibrated with gel-filtration buffer, and the column was run with gel-filtration buffer on an ÄKTA pure FPLC, collecting 500 μl fractions. Elution fractions taken at 14–15.5 ml, which included an A280 peak at 14.53 ml, were pooled. FPLC trace peak integration was used to estimate the eluate concentration from the extinction coefficient and molecular weight calculated at http://protcalc.sourceforge.net. Protein was aliquoted, snap frozen in liquid nitrogen, and stored at –80°C.

Mini-T6B and mini-T6B_A peptides

Peptides synthesized at purity $\geq$ 95% (GenScript) were resuspended in gel-filtration buffer, snap frozen in liquid nitrogen, and stored at –80 °C.

Target RNAs

The two-site target RNA used exclusively in Figure 1 was generated by in vitro transcription. In a 50 μl reaction, 1 μM top-strand DNA oligodeoxyribonucleotide and 1 μM bottom strand template oligodeoxyribonucleotide (Table S1) were incubated with 5 mM DTT, 8 mM GTP, 3.75 mM ATP, 3.75 mM CTP, 6.5 mM UTP, 40 mM Tris, pH 7.9, 2.5 mM spermidine, 26 mM $MgCl_2$, 0.01% Triton X-100, and 5 μl T7 polymerase (NEB M0251L) at 37°C for 2.5 h. Full-length RNA was purified on a denaturing gel and resuspended in water. 1 pmol of RNA was prepared for 5′ radiolabeling by dephosphorylation in a 20 μl reaction with rSAP (NEB M0371S) per manufacturer instructions. After incubating at 37°C for 30 min, the enzyme was heat inactivated at 70 °C for 5 min, and 1 μl 115 mM DTT, 1 μl ATP [γ-^{32}P], and 1 μl T4 PNK were added.

After incubating at 37°C for 30 min, the reaction was desalted with a P-30 column and labeled RNA was purified on a denaturing gel, adding 15 μg of GlycoBlue (Invitrogen AM9516) as a coprecipitant during EtOH precipitation.

All other target RNAs were chemically synthesized (Table S1, IDT) and purified on denaturing gels. For each target, 1 pmol of purified 5'-OH RNA was radiolabeled with ATP [γ-^{32}P] and T4 PNK enzyme. After incubating at 37°C for 1 h, the reaction was desalted with a P-30 column and labeled RNA was purified on a denaturing gel, adding 20 μg of linear acrylamide (Invitrogen AM9520) as a coprecipitant during EtOH precipitation.

Binding reactions

Unless specified otherwise, binding reactions were performed with 5 pM target RNA in 18 mM HEPES pH 7.4, 100 mM KAc, 1.6 mM MgAc, 0.01 mg/ml yeast tRNA, 0.0029% IGEPAL CA-630, 0.058 mg/ml BSA, and 5 mM DTT. Binding reactions of Fig. 2B, C, F, and I, Fig. 3B and E, and Fig. 4A were performed in 20 mM HEPES pH 7.4, 110 mM KAc, 1.7 mM MgAc, 0.01 mg/ml yeast tRNA, 0.0039% IGEPAL CA-630, 0.058 mg/ml BSA, and 5 mM DTT. Binding reactions of Fig. 4B were performed in 22 mM HEPES pH 7.4, 120 mM KAc, 1.8 mM MgAc, 0.01 mg/ml yeast tRNA, 0.0049% IGEPAL CA-630, 0.058 mg/ml BSA, and 5 mM DTT. For reactions including 6B-ABD and/or mini-T6B, 6B-ABD and mini-T6B were the last components added to the reaction mixture, with mini-T6B added after 6B-ABD in reactions including both. Reactions were incubated at 37°C for 2 h.

Filter Binding

For each binding reaction, a nitrocellulose (Amersham Protran 10600062) and a nylon (Amersham Hybond-XL, catalog number RPN 2020 S) filter-paper disc (0.5 inch diameter) was equilibrated for 1 h in filter-paper equilibration buffer (18 mM HEPES pH 7.4, 100 mM KAc, and 1 mM MgAc). The nitrocellulose disc was then stacked atop the nylon disc, which was placed atop a similar-sized circular pedestal. After applying 100 μl filter-paper equilibration buffer to the filter papers, the pedestal, with filter papers, was placed on a vacuum manifold (Visiprep SPE Vacuum Manifold, Supelco 57250-U) set at ~ −7.5 in Hg. After applying 10 μl of filter-paper equilibration buffer as a blank to ensure proper vacuum suction, 10 μl of the sample was applied to the stacked filter papers. Filter papers were washed with 100 μl ice-cold filter-binding wash buffer (18 mM HEPES pH 7.4, 100 mM KAc, 1 mM MgAc, 5 mM DTT), the pedestal with filter papers was removed from the apparatus, and the filter papers were separated, air dried, and imaged on a phosphorimager (Typhoon FLA 7000 or Typhoon FLA 9500, GE). Images were quantified using Multi Gauge software (Fuji Film) to assess the fraction of target bound by miRNA–AGO2.

To measure the concentration of purified miRNA–AGO2, a titration series of purified miRNA–AGO2 was added to 600 pM target RNA harboring a single 7-nt binding site and a 5′ monophosphate, some of which was radiolabeled. These data were fit to a saturation curve, which was used to infer the concentration of miRNA–AGO2 complex. To measure K_D values, 5 pM RNA was combined with miRNA–AGO2 ranging from 0–600 pM in 10 μl reactions.

EMSA

When analyzing the same binding reaction with both filter binding and an EMSA, 22 μl

of reaction was prepared. 10 μl were used for filter binding, and the remaining sample

was place on ice for. After filter binding of all samples was finished, the portions of

binding reaction that remained were loaded (without loading dye) on a pre-chilled (2 h in

5.5 °C cold room), pre-run (10 min) native acrylamide gel (6% 29:1 acrylamide:bis-

acrylamide, 7.8% glycerol, 89 mM Tris base, 89 mM boric acid, 2 mM EDTA, 18 mM

HEPES pH 7.4, 3 mM $MgCl_2$; running buffer: 89 mM Tris base, 89 mM boric acid, 2 mM

EDTA, 18 mM HEPES pH 7.4, 3 mM $MgCl_2$). When analyzing a binding reaction with

only an EMSA, 11 μl of reaction was prepared, incubated at 37°C for 2 h, placed on ice

for 5 min, and then loaded on the gel. After running at 12 W for 90 min in the cold room,

gels were the disassembled, bottoms of unused flanking wells were marked by adding

radioactive samples, and the gels were exposed on a phosphorimager screen at –20°C

overnight prior to imaging and quantification.

Fitting curves to data

A one-site specific binding curve equation or a specific binding with Hill slope equation

was fit to data using Prism.

Slicing reactions

Reactions included 50 pM 55-nt target, 50 pM 22-nt target, 5 pM miR-1–AGO2, 0 or 1

nM 6B-ABD (which had been preincubated with miR-1–AGO2 at 37°C for 5 min) in 16

mM HEPES pH 7.4, 88 mM KAc, 1.0 mM MgAc, 0.0078 mg/ml yeast tRNA, 0.0017%

IGEPAL CA-630, 0.073 mg/ml BSA, 5 mM DTT. Reactions were incubated 37°C, and at

the indicated time points, 10 μl of reaction was removed and added to 10 μl denaturing loading dye (8 M urea, 25 mM EDTA) and placed on ice. Target and cleaved target were resolved on 15% denaturing gels and quantified using a phosphorimager. Linear curves were fit to fraction cleaved using Prism.

Table S1

Oligo	Description	Sequence
hsa-miR-124 capt s biot	miR-124 capture oligo	mUmCmUmUmCmCmUmCmCmUmCmGmCmCmAmCmAmGmAmAmGmUmGmCmCmUmUmAmAmCmCmUmUmAmCmAmCmAmC/3Bio/
hsa-miR-124 comp	miR-124 competitor oligo	AAGGTTAAGGCACTTCTGTGGCGGAGGAAGA
hsa-miR-1 capt s biot	miR-1 capture oligo	mCmAmCmAmCmAmUmUmCmCmUmAmAmCmCmUmUmAmCmAmUmCmAmCmAmCmUmCmGmCmCmUmCmCmUmUmCmU/3Bio/
hsa-miR-1 comp	miR-124 competitor oligo	AAGGTTGGAATGTGTGGTGGTGCGGAGGAAGA
22.1	hsa-miR-1 mature	rUrGrGrArArUrGrUrArArArGrArArGrUrArUrGrUrArU
22.2	hsa-miR-1 star	/5Phos/rArCrArUrArCrUrUrCrUrUrUrArUrArGrCrCrArU
22.10	hsa-miR-124 mature	rUrArArGrGrCrArCrGrCrGrGrUrGrArArUrGrCrCrArA
22.11	hsa-miR-124 star	/5Phos/rCrGrUrGrUrUrCrArCrArGrCrGrGrArCrCrUrUrGrArU
47.1 IVT RNA synth	1 site, 7mer-m8, short, poly(U), miR-1	rGrGrCrGrUrUrUrUrUrUrUrUrUrUrArCrArUrUrCrCrUrUrUrUrUrU
75.1 IVT RNA synth	2 site, 21 nt spacing, 7mer-m8, poly(U), miR-1	rGrGrCrGrUrUrUrUrUrUrUrUrUrUrArCrArUrUrCrCrUrUrUrUrUrUrUrUrUrUrUrUrUrUrUrUrUrArCrArUrUrCrCrUrUrUrUrUrU
75.14 IVT RNA synth	2 sites, 21 nt spacing, 7mer-m8, poly(U), miR-124	rGrGrCrGrUrUrUrUrUrUrUrUrUrUrUrGrCrCrUrUrUrUrUrUrUrUrUrUrUrUrUrUrUrUrUrGrCrCrUrUrUrUrUrU
75.17 IVT RNA synth	2 site, 21 nt spacing, 7mer-m8, poly(U), miR-124 (site 1), miR-1 (site 2)	rGrGrCrGrUrUrUrUrUrUrUrUrUrUrUrGrCrCrUrUrUrUrUrUrUrUrUrUrUrUrUrUrUrUrArCrArUrUrCrCrUrUrUrUrUrU
114.1 IVT RNA synth	2 site, 60 nt spacing, 7mer-m8, poly(U), miR-1	rGrGrCrGrUrUrUrUrUrUrUrUrUrUrArCrArUrUrCrCrUrUrUrUrUrUrUrUrUrUrUrUrUrUrUrUrUrUrUrUrUrUrUrUrUrUrUrUrUrUrUrUrUrArCrArUrUrCrCrUrUrUrUrUrU
58.2 IVT RNA synth	2 site, 7mer-m8, 4 nt between sites, poly(U), miR-124 (site 1), miR-1 (site 2)	rGrGrCrGrUrUrUrUrUrUrUrUrUrUrGrCrCrUrUrUrUrGrArUrArCrArUrUrCrCrUrUrUrUrUrU
75.11 IVT RNA synth	1 site, 7mer-m8 + perfect, 45 nt cleavage product, miR-1	rUrUrUrUrUrUrArCrArUrUrCrCrUrUrUrUrUrUrUrUrUrUrGrArUrArArCrArUrArCrUrUrCrCrUrUrUrUrArCrArUrUrCrCrArUrUrCrCrA
22.9	1 site, perfect cleavage site, 12 nt cleavage product, miR-1	rArUrArCrArUrArCrUrUrCrUrUrUrArCrArUrUrCrCrA
48.12	TNRC6B aa 162 forward for cloning into pMAL	GGATCCGAATTCCCTGCAGGTAATTCAAATTATGCAAATTCCACTTGG
66.2	TNRC6B through 996, plus His6 tag, for cloning into pMAL	TTCGTTTTATTTGAAGCTTATTTAGTGATGATGATGATGATGTGAGCACTTCATTTGTTTCTTTCC
27.2	pMAL-C5X forward for TNRC6B1-1002His6 Gibson	TAAATAAGCTTCAAATAAAACGAAAGG
20.4	pMAL-C5X reverse for TNRC6B1-1002His6 Gibson	ATTACCTGCAGGGAATTCGG
21.1	T7 IVT top strand	GCGTAATACGACTCACTATAG
75.1	2 sites, 21 nt spacing, 7mer-m8, poly(U), miR-1 DNA template for IVT	AAAAAAGGAATGTAAAAAAAAAAAAAAAAAAAAGGAATGTAAAAAAAAAACGCCTATAGTGAGTCGTATTACGC

Peptide	Description	Sequence
mini-T6B	TNRC6B competitor peptide	LSNTGWGQTQIKQDTVWDIEEVPRPBGKSDEGTEGWESAAT
mini-tT6B_A	TNRC6B competitor peptide, W to A	LSNTGAGQTQIKQDTVADIEEVPRPBGKSDEGTEGAESAAT

References

Bartel, D.P. (2009). MicroRNAs: target recognition and regulatory functions. Cell *136*, 215-233.

Chen, G.R., Sive, H., and Bartel, D.P. (2017). A Seed Mismatch Enhances Argonaute2-Catalyzed Cleavage and Partially Rescues Severely Impaired Cleavage Found in Fish. Molecular cell *68*, 1095-1107 e1095.

Eichhorn, S.W., Guo, H., McGeary, S.E., Rodriguez-Mias, R.A., Shin, C., Baek, D., Hsu, S.H., Ghoshal, K., Villen, J., and Bartel, D.P. (2014). mRNA destabilization is the dominant effect of mammalian microRNAs by the time substantial repression ensues. Molecular cell *56*, 104-115.

Elkayam, E., Faehnle, C.R., Morales, M., Sun, J., Li, H., and Joshua-Tor, L. (2017). Multivalent Recruitment of Human Argonaute by GW182. Molecular cell *67*, 646-658 e643.

Flores-Jasso, C.F., Salomon, W.E., and Zamore, P.D. (2013). Rapid and specific purification of Argonaute-small RNA complexes from crude cell lysates. Rna *19*, 271-279.

Friedman, R.C., Farh, K.K., Burge, C.B., and Bartel, D.P. (2009). Most mammalian mRNAs are conserved targets of microRNAs. Genome research *19*, 92-105.

Grimson, A., Farh, K.K., Johnston, W.K., Garrett-Engele, P., Lim, L.P., and Bartel, D.P. (2007). MicroRNA targeting specificity in mammals: determinants beyond seed pairing. Molecular cell *27*, 91-105.

Hauptmann, J., Schraivogel, D., Bruckmann, A., Manickavel, S., Jakob, L., Eichner, N., Pfaff, J., Urban, M., Sprunck, S., Hafner, M., *et al.* (2015). Biochemical isolation of Argonaute protein complexes by Ago-APP. Proceedings of the National Academy of Sciences of the United States of America *112*, 11841-11845.

Jonas, S., and Izaurralde, E. (2015). Towards a molecular understanding of microRNA-mediated gene silencing. Nature reviews Genetics *16*, 421-433.

Landthaler, M., Gaidatzis, D., Rothballer, A., Chen, P.Y., Soll, S.J., Dinic, L., Ojo, T., Hafner, M., Zavolan, M., and Tuschl, T. (2008). Molecular characterization of human Argonaute-containing ribonucleoprotein complexes and their bound target mRNAs. Rna *14*, 2580-2596.

McGeary, S.E., Lin, K.S., Shi, C.Y., Bisaria, N., and Bartel, D.P. (2018). The biochemical basis of microRNA targeting efficacy. bioRxiv.

Pfaff, J., Hennig, J., Herzog, F., Aebersold, R., Sattler, M., Niessing, D., and Meister, G. (2013). Structural features of Argonaute-GW182 protein interactions. Proceedings of the National Academy of Sciences of the United States of America *110*, E3770-3779.

Saetrom, P., Heale, B.S., Snove, O., Jr., Aagaard, L., Alluin, J., and Rossi, J.J. (2007). Distance constraints between microRNA target sites dictate efficacy and cooperativity. Nucleic acids research *35*, 2333-2342.

Salomon, W.E., Jolly, S.M., Moore, M.J., Zamore, P.D., and Serebrov, V. (2015). Single-Molecule Imaging Reveals that Argonaute Reshapes the Binding Properties of Its Nucleic Acid Guides. Cell *162*, 84-95.

Sheu-Gruttadauria, J., and MacRae, I.J. (2018). Phase Transitions in the Assembly and Function of Human miRISC. Cell *173*, 946-957 e916.

Subtelny, A.O., Eichhorn, S.W., Chen, G.R., Sive, H., and Bartel, D.P. (2014). Poly(A)-tail profiling reveals an embryonic switch in translational control. Nature *508*, 66-71.

Takimoto, K., Wakiyama, M., and Yokoyama, S. (2009). Mammalian GW182 contains multiple Argonaute-binding sites and functions in microRNA-mediated translational repression. Rna *15*, 1078-1089.

Wee, L.M., Flores-Jasso, C.F., Salomon, W.E., and Zamore, P.D. (2012). Argonaute divides its RNA guide into domains with distinct functions and RNA-binding properties. Cell *151*, 1055-1067.

Chapter 3. Future directions

In vitro biochemistry

This dissertation investigated the effect of the TNRC6B AGO-binding domain

(6B-ABD) on the cooperative binding of miRNA–AGO2 to target RNA. Adding 6B-ABD

to miRNA–AGO2 robustly increased the Hill coefficient, *h*, for *in vitro* binding of miRNA–

AGO2 to synthetic target RNA bearing two miRNA target sites that were spaced

sufficiently apart for two miRNA–AGO2 complexes to simultaneously bind. miRNA–

AGO2 binding to target mRNA correlates with mRNA repression and therefore these

data are interpreted as TNRC6 playing an explanatory role in the observation that

closely spaced miRNA sites act to synergistically repress a target mRNA (Grimson et

al., 2007; Saetrom et al., 2007).

Experiments performed focused solely on *in vitro* work with TNRC6B,

investigating the binding of miRNA–AGO2 to synthetic target RNA, in the absence or

presence of 6B-ABD. In human, TNRC6 has three paralogues, TNRC6A–C, and

Argonaute has four paralogues, AGO1–4 (Bartel, 2018; Landthaler et al., 2008). Aside

from differential abilities to slice RNA, AGO proteins are functionally similar and typically

loaded with the same pool of miRNAs (Dueck et al., 2012; Faehnle et al., 2013;

Hauptmann et al., 2013; Nakanishi et al., 2013). TNRC6 proteins are also largely similar

to each other, with grossly overlapping functions and domain structures: an N-terminal

ABD and a C-terminal silencing domain that is responsible for recruiting repressive

machinery (Lazzaretti et al., 2009). The C-terminal domain could have additional impact

on binding of TNRC6 to AGO. For instance, TNRC6 uses tryptophan motifs to interact

with CCR4–NOT and PAN2–PAN3 (Christie et al., 2013; Jonas and Izaurralde, 2015; Mathys et al., 2014). While those domains that recruit deadenylases have not been shown to have strong interactions with AGO, other weak AGO–TNRC6 interactions may occur at these tryptophan residues. It has been shown that full length TNRC6A binds tighter to AGO2 than any of the individual AGO-binding hotspots alone (Elkayam et al., 2017).

While AGO and TNRC6 paralogues are similar to each other, different affinities exist between different AGO–TNRC6 paralogue combinations (Elkayam et al., 2017). Thus, it is possible that different AGO–TNRC6 complexes elicit different cooperative binding profiles. To more fully examine AGO–TNRC6 interactions, *in vitro* EMSA experiments could be carried out using each of the 12 different combinations of AGO1–4 and full length, unmodified, TNRC6A–C to examine how different protein–protein interactions may affect h values.

Additional experiments could further dissect the individual AGO-binding hotspots on TRNC6 and their interactions with AGO proteins. The three AGO-binding hotspots on both TNRC6A and TNRC6B have each been shown to have different affinities for AGO1 and AGO2 protein (Elkayam et al., 2017; Pfaff et al., 2013). Furthermore, the affinity of full length TNRC6A for binding AGO2 changes depending on whether or not AGO is already bound to TNRC6; the first AGO2 protein to bind TNRC6A does so at 7.7 nM affinity and the second AGO2 to bind the same TNRC6A binds at 1000 nM affinity (Elkayam et al., 2017). To add complexity, the K_D values for each of the three AGO-binding hotspots on TNRC6A to AGO2 were measured alone as 120 nM, 47 nM, and

230 nM. Thus, it appears as if full length TNRC6A binding to AGO2 may be affected by additional elements within TNRC6A. To try to further understand these nuances, full length TNRC6 protein could be made with one or two AGO-binding hotspots mutated by changing tryptophan residues to alanine, which is sufficient to prevent AGO–TNRC6 interaction (Pfaff et al., 2013; Sheu-Gruttadauria and MacRae, 2018). One TNRC6 paralogue has three AGO-binding hotspots; to combinatorially mutate 0, 1, 2, or 3 of each of the hotspots yields 2^3, or 8, possible isoforms for each of the three TNRC6 paralogues, or 24 different isoforms total. Isothermal titration calorimetry curves, as performed in published characterizations, could be repeated with each of these 24 TNRC6 AGO-binding-hotspot variants (Elkayam et al., 2017). The values to measure would be affinities for each AGO-binding to each of the hotspot mutation variants. These binding values may shed light on which of the three hotspots is bound first or second, and if hotspot preference varies for AGO or TNRC6 paralogues.

This dissertation showed how two different miRNAs loaded into AGO2 can work in combination with each other and TNRC6 to cooperatively bind target RNA. However, different AGO proteins have not been tested in combination with one another. Therefore, experiments could be performed to look at different AGO proteins working in combination. First, however, AGO1, AGO3, and AGO4 should be tested individually for cooperative binding in the presence of TNRC6, as the cooperative binding of those AGO paralogues has not yet been examined. Based on the fact that each of these proteins has tryptophan-binding pockets with which to bind TNRC6, each AGO would naïvely be expected to be capable of cooperative binding to target (Elkayam et al.,

2012; Nakanishi et al., 2013; Park et al., 2019; Schirle and MacRae, 2012; Sheu-Gruttadauria and MacRae, 2018). After establishing which AGO paralogues are capable of binding target cooperatively, those AGO proteins could be tested in combination with one another. For example, a target RNA would be created with two sites, 21 nt apart, to miR-1 and miR-124. Then, miR-1–AGO1 could be added in combination with miR-124–AGO2 and run on EMSA to look for cooperative binding as seen by a super-shifted band in the presence of TNRC6 as well as a lower fraction of singly bound target.

Furthermore, while these studies in cooperativity have only addressed the binding of two AGO proteins simultaneously to target, TNRC6 has three AGO-binding hotspots (Elkayam et al., 2017; Lazzaretti et al., 2009; Pfaff et al., 2013). Therefore, one molecule of TNRC6 may be able to simultaneously bind three AGO proteins and mediate cooperativity to a greater extent than has been investigated. To see if TNRC6 holds the potential for greater cooperative AGO-binding to target, similar EMSA assays as before could be performed, but with target RNAs harboring three miRNA sites, rather than two. In this case, the maximum theoretical h would be 3. Thus, EMSA assays could be performed and h would be interrogated. One caveat of EMSA is that it may not provide sufficient resolution to distinguish each of the possible target–miRNA–AGO–TNRC6 complexes.

TNRC6A affinity to AGO depends on whether or not AGO is loaded with miRNA; TNRC6A has ~5-8 fold higher affinity to loaded AGO over unloaded AGO (Elkayam et al., 2017). Combined with the fact that unloaded AGO protein is less stable than miRNA–AGO, this decreased affinity for unloaded AGO could be a level of cellular

regulation to help recruit TNRC6 and repressive machinery more selectively to mRNAs designated for degradation (Elkayam et al., 2012). If miRNA–AGO binds to a highly complementary target or to a target with a unique pairing geometry, such a site may cause unloading of AGO or degradation of the miRNA rather than target degradation (Ameres et al., 2010; Cazalla et al., 2010; De et al., 2013; Kleaveland et al., 2018; Sheu-Gruttadauria et al., 2019). The structure of target-directed miRNA degradation (TDMD)-competent highly paired AGO2 has been solved and shows the 3′ end of the miRNA to be more exposed to solvent and cellular enzymes (Sheu-Gruttadauria et al., 2019). An AGO mutant was generated whereby a mutation of one residue within AGO helps expose the 3′ end of the miRNA to solvent and increases tailing and trimming of the miRNA (Sheu-Gruttadauria et al., 2019). That AGO mutant could be used in *in vitro* binding experiments with 6B-ABD to test if the 3′ end exposure conformation might reduce AGO affinity to TNRC6; as that target pairing interaction is more likely to lead to TDMD, such a miRNA site may not have evolved for the purpose of target repression.

An additional avenue of exploration of miRNA cooperativity is the recently characterized AGO phosphorylation cycle wherein AGO protein is differentially phosphorylated depending on miRNA–AGO–target engagement (Golden et al., 2017; Quevillon Huberdeau et al., 2017). AGO is phosphorylated upon target engagement, which reduces affinity for target, causing target disengagement. Then, free miRNA–AGO is dephosphorylated which allows future binding of new target mRNA (Golden et al., 2017). The authors point to the idea that AGO phosphorylation may be stimulated by recruitment of silencing factors, such as CCR4–NOT or DDX6 (Golden et al., 2017).

AGO in different phosphorylation states could be purified from HEK293 cells that are knockouts for either the kinase or phosphatase. This AGO could then be used in ITC assays with purified full length TNRC6 to assess the effects of AGO phosphorylation on TNRC6 engagement, and, by extension, how AGO phosphorylation may affect recruitment of silencing factors to a target mRNA.

In vivo experiments

Transitioning from *in vitro* to *in vivo* perturbations of TNRC6 and/or AGO can answer the question of how cooperative miRNA-mediated target repression is impacted on the transcriptome scale. In order to interrogate cooperative target repression from a TNRC6-centric approach, TNRC6 should be edited at the DNA locus to alter the ABD from three AGO-binding hotspots, to one. It has been shown that overexpressing one AGO-binding hotspot alone, "T6B," in HeLa cells can de-repress miRNA targets (Hauptmann et al., 2015). Overexpressing T6B outcompetes endogenous TNRC6, T6B occupies tryptophan-binding pockets on AGO, but as T6B lacks the C-terminal silencing domain, it cannot recruit repressive machinery, and targets are de-repressed (Hauptmann et al., 2015; Lazzaretti et al., 2009; Zipprich et al., 2009). Thus, in order to maintain mRNA repression but perturb cooperativity, the C-terminus should remain intact. CRISPR could be used to target each of TNRC6A–C at their endogenous loci in a human cell line, such as HEK293; all TNRC6 paralogues would need to be modified to pair the C-terminal silencing domain to one, minimal, AGO-binding hotspot (such a construct is similar to the above *in vitro* experimental to combinatorially generate 24

TNRC6 AGO-binding hotspot isoforms). Then, into this modified cell line ("TNRC6 non-cooperative"), and standard HEK293 cells, a miRNA could be transfected and changes in global RNA levels could be monitored by RNA sequencing. The expected result would be that mRNA targets harboring cooperatively spaced sites to the transfected miRNA would be repressed in both cell lines, but the level of repression would be greater in the wild-type cell line that is known to be capable of cooperative repression than the TNRC6 non-cooperative cell line. These transfection and sequencing data may also prove useful for improving miRNA targeting predictions at cooperatively spaced sites.

An additional aspect of TNRC6 to investigate is the spacing of AGO-binding hotspots on TNRC6 in relation to the miRNA site spacing parameters competent for cooperative target repression. As discussed in the previous chapter of this dissertation, *in vitro* experiments did not space miRNA sites far apart enough that they no longer elicited cooperative binding of miRNA–AGO–TNRC6 to target. Previous work found that the optimal distance for cooperative repression of target is either 8–39 or 13–35 nt between the 3' end of the first site and the 5' end of the second site (Grimson et al., 2007; Saetrom et al., 2007). The *in vitro* conditions and purified RNA and protein used did not contain the variety of other proteins found in cytosol that may impede cooperative action of sites spaced at a distance. While *in vivo* and *in vitro* miRNA sites spaced very closely together are simply unable to sterically accommodate the simultaneous binding of two miRNA–AGO, sites that are spaced too far apart *in vivo* may be beyond the flexible reach of TNRC6. Therefore, CRISPR could be used to edit

the ABD of TNRC6 to increase the distance between AGO-binding hotspots. For simplicity, a cell line could be created with TNRC6A and TNRC6C knocked out via CRISPR. Then, TNRC6B could either be left in its endogenous form, or CRISPR could be further used to duplicate the sequence between ABDs, thereby doubling the distance between each ABD ("TNRC6B–long").

Into the TNRC6B-only cell line and the TNRC6B–long cell line, a miRNA would be transfected and, post-transfection, mRNA would be sequenced. The expectation would be that the TNRC6B-only cell line would be able to cooperatively repress targets in line with the previously published cooperative site spacing distances. The TNRC6B–long cell line would also cooperatively repress targets, but the optimal site spacing distance for cooperativity would be different, with a higher upper-bound. While distance between ABDs would be doubled in the experiment, the miRNA site spacing would not necessarily be doubled, as sequence space and three-dimensional space are not expected to correspond at a 1:1 ratio. Rather, in TNRC6B–long, there may be a modest increase in the upper bound of effective cooperative distances between miRNA sites.

In conclusion, in the instance in which two miRNA sites are located proximal to each other on the same mRNA transcript, and those two miRNAs are simultaneously expressed, TNRC6 acts to slow the dissociation rate of miRNA–AGO from target RNA, causing those miRNAs to synergistically repress the target. Further studies could tease apart the different TNRC6 paralogues, their AGO-binding hotspots, and each of those hotspots' interactions with each AGO paralogue. Working *in vivo* would help to assess the effects of TNRC6 on cooperative repression on the transcriptome-wide scale.

References

Ameres, S.L., Horwich, M.D., Hung, J.H., Xu, J., Ghildiyal, M., Weng, Z., and Zamore, P.D. (2010). Target RNA-directed trimming and tailing of small silencing RNAs. Science *328*, 1534-1539.

Bartel, D.P. (2018). Metazoan MicroRNAs. Cell *173*, 20-51.

Cazalla, D., Yario, T., and Steitz, J.A. (2010). Down-regulation of a host microRNA by a Herpesvirus saimiri noncoding RNA. Science *328*, 1563-1566.

Christie, M., Boland, A., Huntzinger, E., Weichenrieder, O., and Izaurralde, E. (2013). Structure of the PAN3 pseudokinase reveals the basis for interactions with the PAN2 deadenylase and the GW182 proteins. Molecular cell *51*, 360-373.

De, N., Young, L., Lau, P.W., Meisner, N.C., Morrissey, D.V., and MacRae, I.J. (2013). Highly complementary target RNAs promote release of guide RNAs from human Argonaute2. Molecular cell *50*, 344-355.

Dueck, A., Ziegler, C., Eichner, A., Berezikov, E., and Meister, G. (2012). microRNAs associated with the different human Argonaute proteins. Nucleic acids research *40*, 9850-9862.

Elkayam, E., Faehnle, C.R., Morales, M., Sun, J., Li, H., and Joshua-Tor, L. (2017). Multivalent Recruitment of Human Argonaute by GW182. Molecular cell *67*, 646-658 e643.

Elkayam, E., Kuhn, C.D., Tocilj, A., Haase, A.D., Greene, E.M., Hannon, G.J., and Joshua-Tor, L. (2012). The structure of human argonaute-2 in complex with miR-20a. Cell *150*, 100-110.

Faehnle, C.R., Elkayam, E., Haase, A.D., Hannon, G.J., and Joshua-Tor, L. (2013). The making of a slicer: activation of human Argonaute-1. Cell reports *3*, 1901-1909.

Golden, R.J., Chen, B., Li, T., Braun, J., Manjunath, H., Chen, X., Wu, J., Schmid, V., Chang, T.C., Kopp, F., *et al.* (2017). An Argonaute phosphorylation cycle promotes microRNA-mediated silencing. Nature *542*, 197-202.

Grimson, A., Farh, K.K., Johnston, W.K., Garrett-Engele, P., Lim, L.P., and Bartel, D.P. (2007). MicroRNA targeting specificity in mammals: determinants beyond seed pairing. Molecular cell *27*, 91-105.

Hauptmann, J., Dueck, A., Harlander, S., Pfaff, J., Merkl, R., and Meister, G. (2013). Turning catalytically inactive human Argonaute proteins into active slicer enzymes. Nature structural & molecular biology *20*, 814-817.

Hauptmann, J., Schraivogel, D., Bruckmann, A., Manickavel, S., Jakob, L., Eichner, N., Pfaff, J., Urban, M., Sprunck, S., Hafner, M., *et al.* (2015). Biochemical isolation of Argonaute protein complexes by Ago-APP. Proceedings of the National Academy of Sciences of the United States of America *112*, 11841-11845.

Jonas, S., and Izaurralde, E. (2015). Towards a molecular understanding of microRNA-mediated gene silencing. Nature reviews Genetics *16*, 421-433.

Kleaveland, B., Shi, C.Y., Stefano, J., and Bartel, D.P. (2018). A Network of Noncoding Regulatory RNAs Acts in the Mammalian Brain. Cell *174*, 350-362 e317.

Landthaler, M., Gaidatzis, D., Rothballer, A., Chen, P.Y., Soll, S.J., Dinic, L., Ojo, T., Hafner, M., Zavolan, M., and Tuschl, T. (2008). Molecular characterization of

human Argonaute-containing ribonucleoprotein complexes and their bound target mRNAs. Rna *14*, 2580-2596.

Lazzaretti, D., Tournier, I., and Izaurralde, E. (2009). The C-terminal domains of human TNRC6A, TNRC6B, and TNRC6C silence bound transcripts independently of Argonaute proteins. Rna *15*, 1059-1066.

Mathys, H., Basquin, J., Ozgur, S., Czarnocki-Cieciura, M., Bonneau, F., Aartse, A., Dziembowski, A., Nowotny, M., Conti, E., and Filipowicz, W. (2014). Structural and biochemical insights to the role of the CCR4-NOT complex and DDX6 ATPase in microRNA repression. Molecular cell *54*, 751-765.

Nakanishi, K., Ascano, M., Gogakos, T., Ishibe-Murakami, S., Serganov, A.A., Briskin, D., Morozov, P., Tuschl, T., and Patel, D.J. (2013). Eukaryote-specific insertion elements control human ARGONAUTE slicer activity. Cell reports *3*, 1893-1900.

Park, M.S., Araya-Secchi, R., Brackbill, J.A., Phan, H.D., Kehling, A.C., Abd El-Wahab, E.W., Dayeh, D.M., Sotomayor, M., and Nakanishi, K. (2019). Multidomain Convergence of Argonaute during RISC Assembly Correlates with the Formation of Internal Water Clusters. Molecular cell.

Pfaff, J., Hennig, J., Herzog, F., Aebersold, R., Sattler, M., Niessing, D., and Meister, G. (2013). Structural features of Argonaute-GW182 protein interactions. Proceedings of the National Academy of Sciences of the United States of America *110*, E3770-3779.

Quevillon Huberdeau, M., Zeitler, D.M., Hauptmann, J., Bruckmann, A., Fressigne, L., Danner, J., Piquet, S., Strieder, N., Engelmann, J.C., Jannot, G., *et al.* (2017). Phosphorylation of Argonaute proteins affects mRNA binding and is essential for microRNA-guided gene silencing in vivo. The EMBO journal *36*, 2088-2106.

Saetrom, P., Heale, B.S., Snove, O., Jr., Aagaard, L., Alluin, J., and Rossi, J.J. (2007). Distance constraints between microRNA target sites dictate efficacy and cooperativity. Nucleic acids research *35*, 2333-2342.

Schirle, N.T., and MacRae, I.J. (2012). The crystal structure of human Argonaute2. Science *336*, 1037-1040.

Sheu-Gruttadauria, J., and MacRae, I.J. (2018). Phase Transitions in the Assembly and Function of Human miRISC. Cell *173*, 946-957 e916.

Sheu-Gruttadauria, J., Pawlica, P., Klum, S.M., Wang, S., Yario, T.A., Schirle Oakdale, N.T., Steitz, J.A., and MacRae, I.J. (2019). Structural Basis for Target-Directed MicroRNA Degradation. Molecular cell.

Zipprich, J.T., Bhattacharyya, S., Mathys, H., and Filipowicz, W. (2009). Importance of the C-terminal domain of the human GW182 protein TNRC6C for translational repression. Rna *15*, 781-793.

Curriculum vitae

Daniel Briskin

EDUCATION

Massachusetts Institute of Technology, Cambridge, Massachusetts   August 2014–Fall 2019
  PhD, Biology
Ohio State University, Columbus, Ohio   September 2009–June 2012
  Bachelor of Science, Molecular Genetics, Graduated *Summa Cum Laude* with Honor in Arts and
  Sciences

RESEARCH EXPERIENCE

MIT/Whitehead Institute/Howard Hughes Medical Institute, Cambridge, Massachusetts
  June 2015–September 2019
  Principal Investigator: Dr. David P. Bartel, PhD
  Department of Biology
  Description: Investigating cooperativity of miRNA target repression
The Rockefeller University/ Howard Hughes Medical Institute, New York, New York
  September 2012–August 2014
  Principal Investigator: Dr. Thomas Tuschl, PhD
  Laboratory of RNA Molecular Biology
  Description: Developing novel RNA sequencing library preparation technique, generating barcoded
  small RNA libraries, curating miRNA databases
Ohio State University Medical Center, Columbus, Ohio
  January 2011–August 2012
  Principal Investigator: Dr. Carlo M. Croce, MD
  Department of Molecular Virology, Immunology and Medical Genetics; Comprehensive Cancer
  Center
  Description: Investigated roles of miRNAs in breast cancer via mouse models

PUBLICATIONS

- **Briskin, D.,** Bartel, D.P. The biochemical basis for the cooperative action of microRNAs. In preparation.
- La Rocca, G., Olejniczak, S.H., Gonzalez, A.J., **Briskin, D.,** Vidigal, J.A., Spraggon, L., DeMatteo, R.G., Radler, M.R., Lindsten, T., Ventura, A., Tuschl, T., Leslie, C.S., Thompson, C.B. (2015). In vivo, Argonaute-bound microRNAs exist predominantly in a reservoir of low molecular weight complexes not associated with mRNA. **Proceedings of the National Academy of Sciences of the United States of America** 112, 767-772. PMID: 25568082
- Lai, J. Y., Luo, J., O'Connor, C., Jing, X., Nair, V., Ju, W., Randolph, A., Ben-Dov, I. Z., Matar, R. N., **Briskin, D.,** Zavadil, J., Nelson, R. G., Tuschl, T., Brosius, F. C., 3rd, Kretzler, M., Bitzer, M. (2015). MicroRNA-21 in Glomerular Injury. **Journal of the American Society of Nephrology** 26, 805-816, PMID: 25145934
- Wang, X., Wang, H.K., Li, Y., Hafner, M., Banerjee, N.S., Tang, S., **Briskin, D.,** Meyers, C., Chow, L.T., Xie, X., Tuschl, T., Zheng, Z. M. (2014). microRNAs are biomarkers of oncogenic human papillomavirus infections. **Proceedings of the National Academy of Sciences of the United States of America** 111, 4262-4267. PMID: 24591631
- Lai, J.Y., Luo, J., O'Connor, C., Jing, X., Nair, V., Ju, W., Randolph, A., Ben-Dov, I.Z., Matar, R.N., **Briskin, D.,** Zavadil, J., Nelson, R.G., Tuschl, T., Brosius, F.C. 3rd, Kretzler, M., Bitzer, M. (2015). MicroRNA-21 in glomerular injury. **J Am Soc Nephrol** 26, 805-816. PMID: 25145934
- Karaca, E., Weitzer, S., Pehlivan, D., Shiraishi, H., Gogakos, T., Hanada, T., Jhangiani, S.N.,

Wiszniewski, W., Withers, M., Campbell, IM., Erdin, S., Isikay, S., Franco, L.M., Gonzaga-Jauregui, C., Gambin, T., Gelowani, V., Hunter, J.V., Yesil, G., Koparir, E., Yilmaz, S., Brown, M., **Briskin, D.,** Hafner, M., Morozov, P., Farazi, T.A., Bernreuther, C., Glatzel, M., Trattnig, S., Friske, J., Kronnerwetter, C., Bainbridge, M.N., Gezdirici, A., Seven, M., Muzny, D.M., Boerwinkle, E., Ozen, M.; Baylor Hopkins Center for Mendelian Genomics, Clausen, T., Tuschl, T., Yuksel, A., Hess, A., Gibbs, R.A., Martinez, J., Penninger, J.M., Lupski, J.R. (2014). Human CLP1 mutations alter tRNA biogenesis, affecting both peripheral and central nervous system function. **Cell** 157, 636-650. PMID: 24766809
- Mosquera, J.M., Sboner, A., Zhang, L., Chen, C.L., Sung, Y.S., Chen, H.W., Agaram, N.P., **Briskin, D.**, Basha, B.M., Singer, S., Rubin, M.A., Tuschl, T., Antonescu, C.R. (2013). Novel MIR143-NOTCH fusions in benign and malignant glomus tumors. **Genes Chromosomes Cancer** 52, 1075-1087. PMID: 23999936
- Nakanishi, K., Ascano, M., Gogakos, T., Ishibe-Murakami, S., Serganov, A.A., **Briskin, D.,** Morozov, P., Tuschl, T., and Patel, D.J. (2013). Eukaryote-specific insertion elements control human ARGONAUTE slicer activity. **Cell reports** 3, 1893-1900. PMID: 23809764
- Di Leva, G., Piovan, C., Gasparini, P., Ngankeu, A., Taccioli, C., **Briskin, D.**, Cheung, D.G., Bolon, B., Anderlucci, L., Alder, H., Nuovo, G., Li, M., Iorio, M.V., Galasso, M., Santhanam, R., Marcucci, G., Perrotti, D., Powell, K.A., Bartasz, A., Garofalo, M., Nephew, K.P., Croce, C.M. (2013). Estrogen mediated-activation of miR-191/425 cluster modulates tumorigenicity of breast cancer cells depending on estrogen receptor status. **PLoS genetics** 9, e1003311. PMID: 23505378
- Di Leva, G., **Briskin, D.**, and Croce, C.M. (2012). MicroRNA in cancer: new hopes for antineoplastic chemotherapy. **Upsala journal of medical sciences** 117, 202-216. PMID: 22348396

TEACHING
- Fall 2018: TA, General biochemistry (7.05), MIT
- Fall 2016: TA, Introductory biology (7.016), MIT

HONORS AND AWARDS
- College of Arts and Sciences Certificate for Excellence in Scholarship – 2012, awarded to outstanding graduating seniors
- Sharp Scholarship for Natural Sciences – 2011-2012, merit-based scholarship
- Ohio State Dean's List – 2009-2012
- Provost Scholarship – 2009-2012, merit-based scholarship